CSIAM Trans. Life Sci.
doi: 10.4208/csiam-ls.SO-2024-0004

Vol. **1**, No. 1, pp. 93-133
March 2025

Advancements in Mathematical Approaches for Deciphering Deep Brain Stimulation: A Systematic Review

Luan Yang[1], Jingdong Zhang[1,2], Shijie Zhou[1,4] and Wei Lin[1,2,3,4,*]

[1] *Research Institute of Intelligent Complex Systems, Fudan University, Shanghai 200433, China.*
[2] *School of Mathematical Sciences, Shanghai Center for Mathematical Sciences, and LMNS, Fudan University, Shanghai 200433, China.*
[3] *MOE Frontiers Center for Brain Science, Institutes of Brain Science, Fudan University, Shanghai 200032, China.*
[4] *Shanghai Artificial Intelligence Laboratory, Shanghai 200232, China.*

Received 28 May 2024; Accepted 31 July 2024

Abstract. Deep brain stimulation (DBS) is a prominent therapy for neurodegenerative disorders, particularly advanced Parkinson's disease (PD), offering relief from motor symptoms and lessening dependence on dopaminergic drugs. Yet, theoretically comprehending either DBS mechanisms or PD neurophysiology remains elusive, highlighting the importance of neuron modeling and control theory. Neurological disorders ensues from abnormal synchrony in neural activity, as evidenced by abnormal oscillations in the local field potential (LFP). Complex systems are typically characterized as high-dimensional, necessitating the application of dimensional reduction techniques pinpoint pivotal network tipping points, allowing mathematical models delve into DBS effectiveness in countering synchrony within neuronal ensembles. Although the traditional closed-loop control policies perform well in DBS technique research, computational and energy challenges in controlling large amounts of neurons prompt investigation into event-triggered strategies, subsequently machine learning emerges for navigating intricate neuronal dynamics. We comprehensively review mathematical foundations, dimension reduction approaches, control theory and machine learning methods in DBS, for thoroughly understanding the mechanisms of brain disease and proposing potential applications in the interdisciplinary field of clinical treatment, control, and artificial intelligence.

AMS subject classifications: 00A71, 97P70, 68T05

Key words: Deep brain stimulation, neuronal network, dimension reduction, control theory, machine learning.

*Corresponding author. *Email addresses:* wlin@fudan.edu.cn (W. Lin), sj_zhou@fudan.edu.cn (S. Zhou)

1 Introduction

Increasing evidence suggests that both invasive and non-invasive modalities [14, 27, 36, 57, 109] of brain stimulation present viable therapeutic avenues for addressing neurodegenerative disorders. Deep brain stimulation stands as the gold standard therapy for neurodegenerative disorders, notably advanced Parkinson's disease [4, 128]. The therapeutic efficacy of DBS often yields remarkable outcomes, ameliorating parkinsonian motor symptoms while concurrently reducing reliance on dopaminergic medications [96,97]. Nevertheless, the underlying mechanism through which DBS operates and the complete neurophysiological underpinnings of Parkinson's disease remain incompletely understood. Thus, the realms of neuron modeling and control theory assume substantial significance in deciphering the fundamental mechanisms governing DBS.

The brain, an intricately structured entity, emerges as a complex hierarchical network of interconnected neuronal networks [9, 70, 135]. Neurons assemble into distinct neuronal ensembles, whose interplay engenders larger, more complex assemblies [40,44,112]. While considerable insight has been garnered into the microscopic scale regarding the dynamics of individual neurons, the understanding of macroscopic behavior of such interacting populations of neurons remains extremely limited. It is widely postulated that the functional and information processing capabilities of the brain, spanning from basic perception to the realms of consciousness, emanate from the emergent collective dynamics of these neuronal assemblies. The basal ganglia circuit [20], comprised of pivotal nuclei such as the subthalamic nucleus (STN) and the internal segment of the globus pallidus (GPi), assumes a critical role in the expression of movement disorder. Ongoing endeavors are directed towards addressing dysfunction within this circuit, as a foundational strategy for the design and implementation of DBS.

Symptoms of various neurological disorders, such as PD, are believed to stem from overly synchronous activity within neural ensembles. The severity of clinical impairment in PD is widely recognized to correspond with an increase in the beta (13-15 Hz) oscillations in the local field potential (LFP) and in the activity of individual neurons within the basal ganglia circuit [102]. Simultaneously, abnormal synchrony patterns are associated with malfunction in disorders such as epilepsy and PD [123]. Biological and neural systems can be seen as networks of interacting periodic processes. A computational network model of the STN and the GPi within the indirect pathway of the basal ganglia can be aptly characterized by the Hodgkin-Huxley (HH) model [102].

The human brains comprises a multitude of dynamical units, this naturally and urgently calls for developing efficient methods for properly extracting and quantifying the collective behavior of the complex spatio-temporal dynamics of neuronal oscillators. Although the dimensional reduction for large-scale neural oscillators from the perspective of clinical experiments have been comprehensively investigated [41, 103], theoretical dimensional reduction of the complex mathematical formulation of neuronal dynamics still remains a gap. The basic idea of dimensional reduction is to replace the original high-

dimensional dynamics with some low-dimensional dynamics that preserve key features of the original dynamics. We review two major kind of reduction approaches including phase reduction and dimension reduction. In phase reduction scenarios, we aim at simplifying the description of d-dimensional dynamics for each oscillator to a scalar phase dynamics. Hence, we reduce the dN-dimensional dynamics with N interacting oscillatory oscillators to N-dimensional dynamics. In dimension reduction scenarios, the main purpose is to collapse the networked dynamics with N nodes into a simplified version with $n \ll N$ effective dimensions and use it to detect the tipping point of the original network [31].

Numerous mathematical models have been devised to explore DBS methodologies aimed at the synchronization-induced psychiatric disorders through the elimination of the synchrony among oscillatory neuronal ensembles. The feedback control scheme with or without delays [91, 100] performs well in the DBS tasks, nonetheless, continuously monitoring the brain state of patients and updating the control signal with fixed frequency incur large computational burden, and may accumulate too much energy to patients. To alleviate the problem, event-triggered control is suggested as a energy-saving surrogate of feedback control, which updates the control signal at the instants when the current measurement vanish a predefined event function, thereby decreasing the number of control renewals under suitable event function [45].

The neuronal dynamics are generally high-dimensional and highly nonlinear because of the complex interaction between large amounts of brain neurons. Therefore, traditional control methods depending on delicate design of auxiliary functions and rigorous mathematical analysis fail in this setting. As the growth of artificial intelligence (AI), the machine-learning-based control method plays an ever more pivotal role in solving high-dimensional complex tasks in cybernetics [104]. In this review, we consider two types of control problems in neuronal systems: optimal control and stabilization control, both studied systematically by the classic techniques [60, 120] and improved with machine learning methods in recent advancements [56, 131].

The main topic of this review aims at providing a comprehensive overview of the mathematical models and control theory methods employed in the study of deep brain stimulation technology mechanisms. It also integrates current theoretical advancements to elucidate corresponding technological extensions, culminating in the proposition of prospective avenues for future research endeavors.In the following, we provide an outline how to approach this paper. In Section 2, we review the neuronal models from single neuron to neuronal group and illustrate how single neurons create network dynamics both from biological perspective and biophysical perspective. In Section 3, we introduce the dimensional reduction approaches including phase reduction and dimension reduction. In Section 4, we discuss the control schemes subsuming closed-loop feedback control and event-triggered control from the perspective of feedback. In Section 5, we review the existing AI control methods in DBS and summarize the potential research directions in this field in terms of optimal control and stabilization control.

2 From a single neuron to neuronal network

Symptoms of several neurological disorders, such as PD, are thought to arise from overly synchronous activity within neural populations. The severity of clinical impairment in PD is known to be correlated with an increase in the beta (13-35 Hz) oscillations in the local field potential (LFP) and in the activity of individual neurons in the basal ganglia circuit [102] illustrated in Fig. 1(a). Though it is known that PD is underpinned by neurodegeneration of substantia nigra (SN) dopaminergic neurons and by widespread progressive brain pathology, dysfunction at the neural circuit level remains uncertain.

To date, DBS of the STN or the GPi [42] has recently been recognized as an important form of intervention for alleviating motor symptoms associated with Parkinson's disease, but the mechanism underlying its effectiveness remains unclear. Hence, numerous investigations embark upon modeling from the neuron itself and the brain-circuit of pivotal nuclei, thereby scrutinizing their collective dynamical behaviors. In this section, we firstly embark upon an exploration of the mechanistic modeling of single neuron and synaptic connections, with an elucidation of their applications pertinent to DBS. Given that abnormal collective dynamical behaviors frequently ensue thereafter, we pivot towards a dual elucidation, encompassing both biological and biophysical perspectives on neuron modeling. Such endeavors are underpinned by the premise that investigations into collective behaviors often exhibit favorable attributes conducive to subsequent theoretical analyses and applied research endeavors, thereby affording a broader applicability within the realm of DBS technique research.

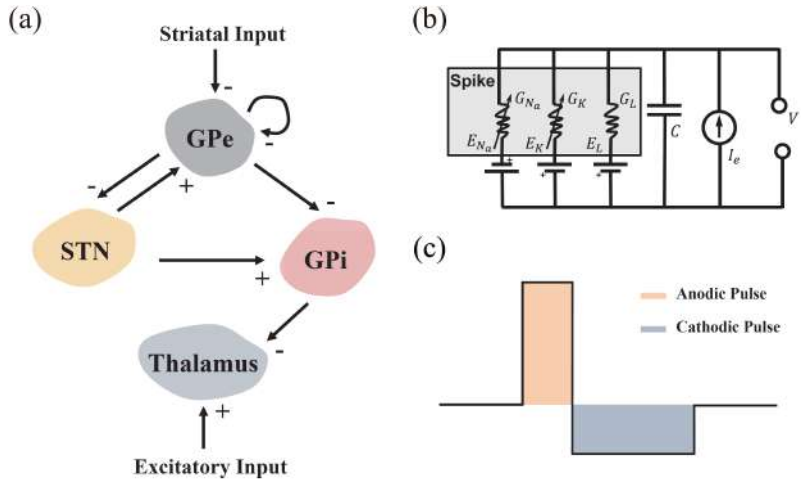

Figure 1: (a) Neuronal structure consists of thalamus, STN, globus pallidus externus (GPe), and GPi. Here, "+" and "-" denote the excitatory and the inhibitory effects, respectively. The STN exhibits an excitatory influence on the other nuclei, whereas the GPe exerts an inhibitory influence on its own and other nuclei, and GPi exerts an inhibitory influence on the thalamus. (b) Equivalent electric circuit representation of the HH neuron model. (c) An overview of the charge-balanced bi-phasic stimulus pulses.

2.1 Model a single neuron

Single neuron can generate and convey information through the interplay of ion channels which have dynamics at different timescales, voltage thresholds and inactivation. Early research often revolved around the HH model [28,48,76,113,114], which provided a foundational framework by simplifying the complex models. Neuronal models are classified as conductance-independent (phenomenological) models, aimed at capturing the neuronal input-output behavior using abstract mathematical language, with minimal concern for the specific physiological structure of neurons. Subsequently, further investigation delved into study neuronal model integrating principles from biophysics and mathematical approximations, FitzHugh-Nagumo (FHN) model [29, 46, 74, 98, 99] and other conductance-dependent (biophysical) models were proposed. These endeavors sought to mirror neuronal behavior by simulating the specific electrophysiological properties of neuronal cell membranes, including the reconstruction of their conductive channels [15]. In this section, we delve into the framework of describing the single neurons by using their action potentials, with particular emphasis on the HH model and the FHN model.

2.1.1 Hodgkin-Huxley model

The Hodgkin-Huxley model, initially devised to simulate the action potential generation in the axon of a giant squid [48], operates through the intricate interplay of dynamical ion channels whose activation and inactivation states depend upon gating variables derived from experiments (see Fig. 1(b)). This model's capability renders it used in evaluating the electrode performance for DBS experiments. The direct experimental assessment of the parameters of the HH model is enabled by the appropriate biophysical levels of abstraction [8,71]. Investigation into axonal responses involves the application of various input stimuli, wherein the shape and the duration of the applied pulses exert notable influence on the initiation of an action potential.

As it base, research delve into modeling cells via the HH model originating from different nuclei. As elucidated in prior studies [102, 119], each cell type is described by single-compartment conductance-based biophysical model within the HH formalism, with membrane currents representative of cells in pivotal nuclei within the basal ganglia circuit. In each instance, the synaptic current $I_{\alpha\to\beta}$ originating from structure α and targeting structure β is defined as

$$I_{\alpha\to\beta}=g_{\alpha\to\beta}[v_\alpha-E_{\alpha\to\beta}]\sum_j s_\alpha^j.$$

Here, $g_{\alpha\to\beta}>0$ is the maximal synaptic conductance, $E_{\alpha\to\beta}$ is the synaptic reversal potential, and s_α^j satisfies the equation of the form

$$s'_\alpha=A_\alpha[1-s_\alpha]H_\infty(v_\alpha-\theta_\alpha)-B_\alpha s_\alpha.$$

Therefore, the neuronal dynamics v_{Th} of the thalamic neurons is governed by

$$\begin{aligned} C_m\dot{v}_{\mathrm{Th}} &= -I_{\mathrm{L}}-I_{\mathrm{Na}}-I_{\mathrm{K}}-I_{\mathrm{T}}-I_{\mathrm{GPi}\to\mathrm{Th}}+I_{\mathrm{SM}}, \\ \dot{h}_{\mathrm{Th}} &= \frac{h_\infty(v_{\mathrm{Th}})-h_{\mathrm{Th}}}{\tau_h(v_{\mathrm{Th}})}, \\ \dot{r}_{\mathrm{Th}} &= \frac{r_\infty(v_{\mathrm{Th}})-h_{\mathrm{Th}}}{\tau_r(v_{\mathrm{Th}})}, \end{aligned} \tag{2.1}$$

where $I_{\mathrm{L}}, I_{\mathrm{Na}}$, and I_{K} represent the leak, the sodium and the potassium currents, respectively. Moreover, I_{T} is a low-threshold calcium current, $I_{\mathrm{GPi}\to\mathrm{Th}}$ represents the input current from GPi to Thalamus, h_{Th} and r_{Th} are the gate variables, and I_{SM} represents sensorimotor input to the thalamus modeled by step function as

$$I_{\mathrm{SM}} = i_{\mathrm{SM}}\cdot H\left(\sin\left(\frac{2\pi t}{\rho}\right)\right)\cdot\left[1-H\left(\sin\left(\frac{2\pi(t+\delta)}{\rho}\right)\right)\right], \tag{2.2}$$

where i_{SM} is the amplitude, H is the typical step function such that

$$H(x)=\begin{cases}0, & x\le 0,\\ 1, & x>0.\end{cases}$$

In addition, ρ is the period of I_{SM} and δ is the duration of the input.

Given that STN represents the frequent focal target in DBS interventions, the modeling of the neural dynamics of STN neurons [119] entails

$$C_m\dot{v}_{\mathrm{STN}} = -I_{\mathrm{L}}-I_{\mathrm{K}}-I_{\mathrm{Na}}-I_{\mathrm{T}}-I_{\mathrm{Ca}}-I_{\mathrm{GPe}\to\mathrm{STN}}+I_{\mathrm{DBS}}, \tag{2.3}$$

where I_{DBS} is modeled as

$$I_{\mathrm{DBS}} = i_{\mathrm{DBS}}\cdot H\left(\sin\left(\frac{2\pi t}{\rho_{\mathrm{DBS}}}\right)\right)\cdot\left[1-H\left(\sin\left(\frac{2\pi(t+\delta_{\mathrm{DBS}})}{\rho_{\mathrm{DBS}}}\right)\right)\right]. \tag{2.4}$$

Here, i_{DBS} corresponds to simulation amplitude, ρ_{DBS} is the stimulation period, and δ_{DBS} represents the duration of each impulse. The specific parameter can be configured based on the strategy employed in DBS therapy [102]. Nevertheless, such unbalanced single-phase stimulation currents may cause side effects on neural tissues [26]. Hence, to mitigate such concerns, a charge-balanced bi-phasic (CBBP) pulses paradigm was proposed. This approach encompasses of short-duration, high amplitude anodic pulse, followed by a long-duration, low amplitude cathodic pulse, as illustrated in Fig. 1(c), which is widely used in surgical DBS procedures.

2.1.2 FitzHugh-Nagumo model

Brain network models offer a framework for simulating and comprehending the human brain as a nonlinear dynamical system. Within such models, each brain region is

conceptualized as a node, with its dynamics governed by a specific dynamical model. The FitzHugh-Nagumo (FHN) model, known for its simplicity relative to the HH model [29,76], is often favored as a representation of nodal dynamics in brain network research. The FHN model is given by

$$\begin{aligned}\frac{\mathrm{d}V}{\mathrm{d}t}&=V-\frac{1}{3}V^3-W+z,\\ \frac{\mathrm{d}W}{\mathrm{d}t}&=\epsilon(V-a+bW),\end{aligned}\tag{2.5}$$

where V is membrane potential, which can generate action potentials through positive feedback, W denotes the recovery variable, regulated by negative feedback to reset the system, and z is the injected current from external environment. The above ordinary differential equations consider the membrane potential only depends on time. When the dissipation of voltage across the membrane is taken into consideration, the spatial-temporal dynamics of a neuron is further modeled by the following partial differential equations (PDEs):

$$\begin{aligned}\frac{\partial V}{\partial t}&=V-\frac{V^3}{3}-W+D\frac{\partial^2 V}{\partial x^2},\\ \frac{\partial W}{\partial t}&=\varepsilon(V+\beta-\gamma W),\end{aligned}\tag{2.6}$$

where D is the diffusion coefficient and can be eliminated by rescaling the space variable, the rate parameter $\epsilon\ll 1$ incurring the membrane potential V and the recovery variable W form the fast-slow dynamics, the parameter set of β and γ renders the neuron excitable without the external stimulation. In [90], the PDE version of the FHN model under high frequency stimulation (HFS) is considered as

$$\begin{aligned}\frac{\partial V}{\partial t}&=V-\frac{v^3}{3}-W+D\frac{\partial^2 V}{\partial x^2}+a\cos(wt),\\ \frac{\partial W}{\partial t}&=\varepsilon(V+\beta-\gamma W),\end{aligned}\tag{2.7}$$

where the HFS is regulated by the parameters a and w.

Utilizing the Liénard transformation, we can transfer the FHN model into the Van der Pol model [52], which can be written in a succinct two-dimensional formulation

$$\begin{aligned}\dot{x}&=y,\\ \dot{y}&=\mu(1-x^2)y-x.\end{aligned}\tag{2.8}$$

This model has been applied in studies concerning the control theory of deep brain stimulation techniques [88].

2.2 Biological perspective

As is commonly acknowledged, a comprehensive investigation into the underlying mechanisms of DBS necessitates the consideration of neuronal circuits. These neural circuits

within the brain exhibit a complex architecture, comprising interconnected populations of neurons, rather than isolated individual units. In this section, we elucidate both 1D dynamical system and 2D dynamical systems which considered both excitatory and inhibitory neurons, whereby the activity are described using firing rate.

2.2.1 Integrate-and-fire model

A straightforward feedforward network [117] is depicted in Fig. 2(a), wherein the postsynaptic neuron generates activity through the integration of the presynaptic inputs u weighted by the matrix m, denoting the strength of the synaptic weights. This yields $I=\sum_{j=1}^{N} m_j u_j$, representing the current encountered by the postsynaptic neuron. Given the linear scaling of presynaptic input units by the postsynaptic neuron, the firing rate activity can be articulated through a differential equation, which reads

$$\tau_r \frac{\mathrm{d}v}{\mathrm{d}t} = -v + F(I) = -v + F(\boldsymbol{m}\cdot\boldsymbol{u}), \tag{2.9}$$

where v is a leak term, τ_r is the time constant, and F is a nonlinear function. Upon extending the feedforward network into encompass multi-postsynaptic neurons (see Fig. 2(b)), then we obtain

$$\tau_r \frac{\mathrm{d}\boldsymbol{v}}{\mathrm{d}t} = -\boldsymbol{v} + F(\boldsymbol{M}\boldsymbol{u}). \tag{2.10}$$

Here, M represents the strength of the connection from a given presynaptic neuron to the postsynaptic neuron.

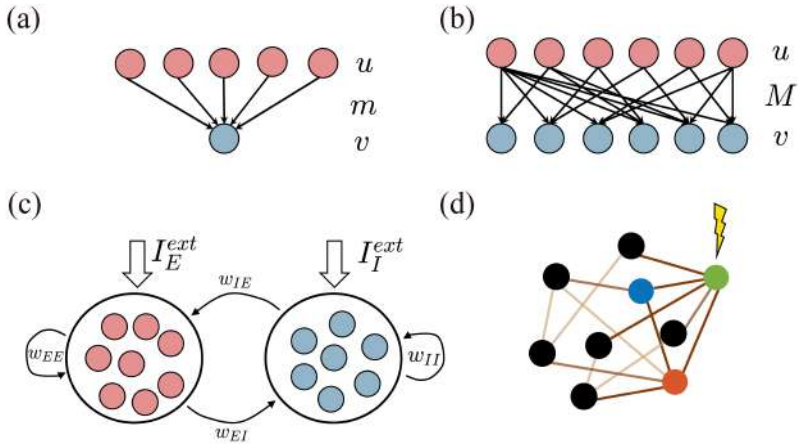

Figure 2: (a) A sketch of the neurons processing the input into the output. Here, u is the activity of the presynaptic neurons, m is the strength of the synaptic weights between the pre- and the postsynaptic neurons, and v is the activity of the postsynaptic neuron. (b) The construction of a feedforward network from multiple presynaptic neurons to multiple post-synaptic neurons. Here, M represents the strength matrix of the synaptic weights between the pre- and postsynaptic neurons. (c) The rate-based model consists of coupled excitatory and inhibitory neuronal populations, where w_{EE} and w_{II} represent the weight matrix of inter-cluster oscillators for each cluster, w_{EI} and w_{IE} are the weight matrix of intra-cluster structure, $I_{\mathrm{E}}^{\mathrm{ext}}$ and $I_{\mathrm{I}}^{\mathrm{ext}}$ are the input current of excitatory population and inhibitory population, respectively. (d) Applying the local stimulation to modulate the neural activity of the target region.

2.2.2 Wilson-Cowan model

In the realms of modeling nuclei within the human brain, the entire postsynaptic neurons can be simplified as a single population, characterized by a single scalar to describe the firing rate of the entire population of neurons due to their similar properties. The entire populations of excitatory and inhibitory neurons can be modeled with the same rate-based equations. These two populations are coupled together (see Fig. 2(c)), then we get the Wilson-Cowan model for a single population of neurons as

$$\begin{aligned}\tau_{\mathrm{E}}\frac{\mathrm{d}r_{\mathrm{E}}}{\mathrm{d}t}&=-r_{\mathrm{E}}+F_{\mathrm{E}}\big(w_{\mathrm{EE}}r_{\mathrm{E}}-w_{EI}r_{\mathrm{I}}+I_{\mathrm{E}}^{\mathrm{ext}}\big),\\ \tau_{I}\frac{\mathrm{d}r_{\mathrm{I}}}{\mathrm{d}t}&=-r_{\mathrm{I}}+F_{\mathrm{I}}\big(w_{\mathrm{IE}}r_{\mathrm{E}}-w_{\mathrm{II}}r_{\mathrm{I}}+I_{\mathrm{I}}^{\mathrm{ext}}\big),\end{aligned}\tag{2.11}$$

where the leaky terms $-r_{\mathrm{E}}$ and $-r_{\mathrm{I}}$ represent the population decay over time subsequent to the removal of the external input. Meanwhile, the cumulative synaptic input into each population is integrated through the nonlinear $F_{\mathrm{E/I}}(\cdot)$ function. Within the exploration of regional stimulation as illustrated in Fig. 2(d), brain regions are conceptualized as nodes within a brain network, whereupon the j-th nucleus can be modeled as

$$\begin{aligned}\tau\frac{\mathrm{d}E_j}{\mathrm{d}t}&=-E_j(t)+\big(S_{\mathrm{E\_max}}-E_j(t)\big)S_{\mathrm{E}}\left(c_1E_j(t)-c_2I_j(t)+c_5\sum_k A_{jk}E_k\big(t-\tau_d^k\big)\right),\\ \tau\frac{\mathrm{d}I_j}{\mathrm{d}t}&=-I_j(t)+\big(S_{\mathrm{I\_max}}-I_j(t)\big)S_{\mathrm{I}}\big(c_3E_j(t)-c_4I_j(t)\big),\end{aligned}\tag{2.12}$$

where $E(t)/I(t)$ represent the firing rate of the excitatory/inhibitory population, respectively, τ signifies a time constant, and $w_j(t)$ and $v_j(t)$ are drawn from a standard normal distribution. Inter-regional interactions are established via the excitatory population, facilitated by a connectivity matrix $\boldsymbol{A}=(A_{ij})$ and time delays denoted by τ_d are derived from real data between brain regions. The transfer function is given by the sigmoidal function

$$S_{\mathrm{E/I}}(x)=\frac{1}{1+\mathrm{e}^{(-a_{\mathrm{E/I}}(x-\theta_{\mathrm{E/I}}))}}-\frac{1}{1+\mathrm{e}^{a_{\mathrm{E/I}}\theta_{\mathrm{E/I}}}}.\tag{2.13}$$

Building upon this framework, we can proceed to intricately examine the dynamical behavior of the entire system under regional stimulation in the presence of both stimulation and external noise [75].

2.3 Biophysical perspective

One of the most prominent collective phenomena observed in an oscillator network is the emergence of nodes synchronization and oscillation in unison. Therefore, the modeling of the disorder diseases can be approached by leveraging the biophysical properties of the system, through the imposition of a phase model such as the Kuramoto model or a network of theta neurons. Neurons are typically classified into two categories due to

different firing patterns and threshold properties, based on the nature of the onset of spiking as a constant injected current exceeds an effective threshold [47, 49]. Type-I neurons exhibits continuous evolution of membrane potential during an action potential, initiating spiking at an arbitrarily low rate, whereas Type-II neurons display a more abrupt transition, commencing spiking activity at a non-zero rate immediately upon threshold is exceeded. From a neurophysiological standpoint, excitatory pyramidal neurons are often categorized as Type-I, while fast-spiking inhibitory interneurons commonly belong to Type-II [79]. Near the spiking onset, Type-I neurons are conceptually modeled as theta neurons [66], and an exemplary model representing Type-II neurons is the Kuramoto model [6].

2.3.1 The theta neuron

The phase equation of theta neuron is modeled as

$$\dot{\theta} = (1-\cos\theta) + (1+\cos\theta)\eta, \tag{2.14}$$

where θ is a phase variable on the unit circle and η is a bifurcation parameter related to the injected current. For $\eta < 0$, the neuron is attracted to a stable equilibrium which represents the resting state illustrated in Fig. 3(a). An unstable equilibrium is also present, representing the threshold. If an external stimulus pushes the neuron's phase across the unstable equilibrium, θ moves around the circle and approaches the resting equilibrium from the other side. When θ crosses $\theta = \pi$, the neuron is said to have spiked [23].

We formulate a cluster of N theta neurons as follows:

$$\dot{\theta}_j = (1-\cos\theta_j) + (1+\cos\theta_j)[\eta_j + I_{\text{syn}}], \tag{2.15}$$

where θ_j is the state of the j-th neuron with the index $j \in \{1,\dots,N\}$. Moreover, the coupling term $I_{\text{syn}} = (k/N)\sum_{i=1}^{N} P_n(\theta_i)$, where $P_n(\theta) = a_n(1-\cos\theta)^n$ with $n \in \mathbb{N}$ and the normalization constant

$$a_n = \frac{2\pi}{\displaystyle\int_{-\pi}^{\pi} \big(1-\cos(x)\big)^n \mathrm{d}x} = \frac{2^{n-1}B(n+1/2,1/2)}{\pi}$$

such that

$$\int_0^{2\pi} P_n(\theta)\mathrm{d}\theta = 2\pi. \tag{2.16}$$

Here, $B(\cdot,\cdot)$ denotes the Beta function, $P_n(\theta)$ becomes more and more sharply peaked as n increases, and k represents the synaptic strength considered the same for all neurons. In Fig. 3(b), the blue circle delineated by dashed lines represent the oscillator in stable state. With couplings, the oscillators rotate along the unit cycle synchronized as shown in Fig. 3(c). The macroscopic behaviour of the theta network is defined by the order parameter

$$z(t) \triangleq \sum_{j=1}^{N} \mathrm{e}^{\mathrm{i}\theta_j}, \tag{2.17}$$

where $|z(t)| \in [0,1]$ represents the extent of synchronization at time t.

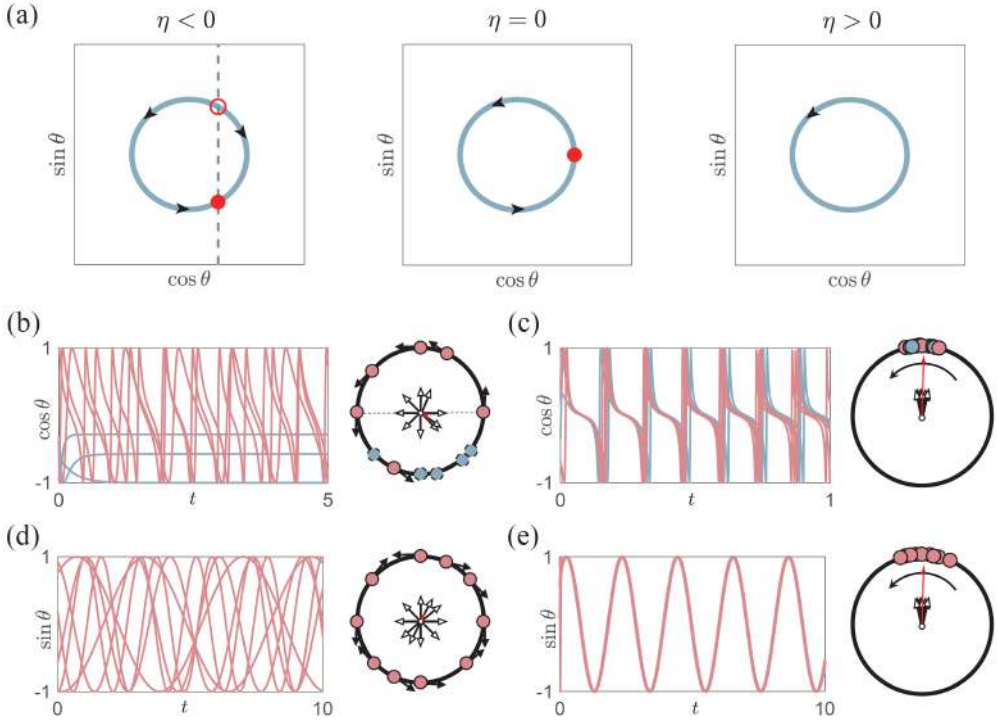

Figure 3: (a) The system (2.14) experiences a Saddle-Node Infinite Periodic Cycle bifurcation as η increases from $0-$ to $0+$. When $\eta<0$, the system exhibits two equilibria: one is stable (represented by a solid red point), while the other is unstable (hollow red point). Both equilibria lie on a vertical line and shift towards the right simultaneously as η increases. The two equilibria coincide at $(1,0)$ when $\eta=0$. In this case, any trajectory moves counterclockwise to $(1,0)$ when $t\to\pm\infty$. For $\eta>0$, the equilibria disappear. The trajectory of the system moves around the unit circle periodically with a period $T=\int_0^{2\pi}[(1+\eta)+(\eta-1)\cos\theta]^{-1}\mathrm{d}\theta$. Dynamics of a cluster of the theta neurons governed by (2.15) for $k=0$ (without coupling, b) and for $k>0$ (with coupling, c). The blue points correspond to the instances where $\eta_i<0$, indicating equilibrium states in the absence of coupling. However, when coupling is present, these points exhibit synchronized movement alongside red points, which correspond to the instances where $\eta_i>0$. Similarly, system (2.21) shows unsynchronized dynamics without coupling (d) and shows synchronized dynamics with coupling (e). The red arrows in (b)-(e) represent the order parameter defined in (2.16) or (2.20).

2.3.2 From Stuart-Landau oscillator to Kuramoto model

Self-oscillating oscillator refers to a system capable of sustaining self-sustained oscillations in the absence of external forces. In study of the synchronized self-oscillating oscillators, researchers have observed the instances where, in spite of variations in amplitude among individual oscillators, their phases remain coherent. This observation has led to the conceptualization of "phase synchronization". Notably, Kuramoto proposed a phase approximation approach to address this phenomenon, wherein equations governing the phases of individual oscillators are approximated. If the behavior of each individual oscillator conforms to the canonical Hopf bifurcation, the classical Kuramoto model emerges.

Initially, we consider the coupled Stuart-Landau (SL) oscillators as follows:

$$\dot{z}_j = \left(\mathrm{i}w_j + 1 - |z_j|^2\right) z_j + KZ, \quad j = 1,2,\ldots,N, \tag{2.18}$$

where z_j represents the dynamics of the j-th oscillator, with w_j denoting its inherent natural frequency. The parameter K is the internal and global coupling strength, while $Z = (1/N)\sum_{j=1}^{N} z_j$ is the mean-field coupling term. Notably, the natural frequencies of each are not identical but obey a specific probability distribution $g(w)$. When $K=0$, each oscillator rotates along with its own natural frequency, thus illustrating a state of unsynchronized dynamics. Letting $z_j = \rho_j \mathrm{e}^{\mathrm{i}\theta_j}$ and $K=0$, we have $\dot{\rho}_j = (1-\rho_j^2)\rho_j$, and then $\rho_j \to 1$, the system (2.18) is rewritten as

$$\dot{\theta}_j = w_j + K \cdot \mathrm{Im}\left\{ r\mathrm{e}^{-\mathrm{i}\theta_j} \right\}, \tag{2.19}$$

where

$$r \triangleq \frac{1}{N}\sum_{j=1}^{N} \mathrm{e}^{\mathrm{i}\theta_j} \tag{2.20}$$

is the order parameter, and $\mathrm{Im}\{\cdot\}$ represents the imaginary part of a given complex number. From a physical perspective, r is the centroid of the coupled oscillators. Therefore, system (2.19) can be written as

$$\dot{\theta}_j = w_j + \frac{K}{N}\sum_{i=1}^{N} \sin(\theta_i - \theta_j), \tag{2.21}$$

which becomes the traditional Kuramoto model. For sufficiently large K [59, 91, 100], system (2.21) shows phase synchronization.

Finally, we explain the physical meaning of order parameter in detail because this amount is widely used in mathematical analysis of neuronal dynamics. The values of $|r|$ vary in the interval $[0,1]$. In the desynchronization state, the phase θ_i are uniformly distributed over the interval $[0,2\pi]$, which corresponds to a nearly zero value for r (see Figs. 3(b,d)). Conversely, in the synchronization state, the phase θ_i are highly concentrated around a single value, leading to being close to 1 (see Figs. 3(c,e)). Consequently, small values of $|r|$ signify the desynchronization state, whereas values of $|r|$ close to 1 signify synchronization state. Therefore, we may employ $|r|$ as a metric to describe the degree of synchronization.

3 Reduction methods for coupled oscillators

Due to the complicated interaction between a large number of nodes in the network, the task of investigating the networked dynamics is not trivial. Therefore, a common choice is to reduce the original high-dimensional dynamics to some low-dimensional dynamics that preserve major information of the original dynamics. There are two major kind of reduction methods, viz., phase reduction and dimension reduction. In phase reduction

scenarios, the major idea is to simplify the description of n-dimensional dynamics for each oscillator to a one-dimensional phase dynamics, thus the evolution on the stable limit-cycle of each oscillator is determined by a single periodic phase variable [6]. In this setting, biologically relevant information is captured by the phase dynamics which are easier to analyze and assess. In dimension reduction scenarios, the main purpose is to collapse the N-dimensional networked dynamics into a simplified version with $n \ll N$ effective dimensions and use it to predict the global activity of the original network [31]. In addition to the dynamics, the network structure plays a pivotal role in this case. Below we summarize the phase reduction and dimension reduction based methods in DBS, and further discuss the potential directions in this field.

3.1 Phase reduction

Delivering stimulation to the ventrolateral thalamus is an common clinical treatment to suppress the patient's symptom. To determine the timing of updating the stimulation, phase dynamics can be set as an effective indicator. H. Cagnan *et al.* [10] employ the band-pass signal from the dominant tremor axis to calculate the phase of tremor, once the real time phase arrives a patient-specific certain threshold, a transistor-transistor logic (TTL) pulse is sent to the patient, which gives rise to tremor suppression. In addition to the phase-specific stimulation, researchers have showed that PD is associated with exaggerated coupling between the phase of beta oscillations and the amplitude of broadband activity in the primary motor cortex, in which the phase-amplitude coupling (PAC) is a phenomenon observed in neural oscillations where the amplitude of high-frequency oscillations is modulated by the phase of low-frequency oscillations [18]. Therefore, an effective way to relax the symptoms of patients is achieved by alleviating excessive beta phase locking of motor cortex neurons [19].

All these previous research demonstrate the efficacy of phase based control in DBS tasks. Nonetheless, a major challenge in applying the phase based control methods into different neuronal oscillators is how to obtain the phase from their original dynamics. In classic coupled oscillator models, neural oscillators correspond to individual neurons described by a set of variables possessing periodic limit-cycle. A mathematical description of such a neuron can be simplified by projecting the state of the neuron on its phase, a one-dimensional scalar variable, which in absence of external input increases with constant frequency from 0 to 2π, corresponding to an evolution of a neuron from spike to spike [3, 7, 126]. Therefore, an effective way to bridge the gap between the clinical treatment and mathematical model is to finding the phase reduction dynamics of general nonlinear neuronal oscillators.

Specifically, we consider the neuronal oscillator under the DBS control as follows:

$$\dot{\boldsymbol{x}} = \boldsymbol{F}(\boldsymbol{x}) + \boldsymbol{u}(\boldsymbol{x}, t), \quad \boldsymbol{x} \in \mathbb{R}^d. \tag{3.1}$$

Here, $\boldsymbol{F}$ is the self-dynamics of the neuron possessing a stable-limit cycle Γ that can incur spike of the neuron, and $\boldsymbol{u}$ is the external forcing representing the DBS stimulation. The

phase function is defined as a periodic function $\theta(\boldsymbol{x}):[0,2\pi)\to\Gamma$ on limit-cycle, and its inverse is denoted as $\boldsymbol{x}^\gamma(\theta):\Gamma\to[0,2\pi)$. In order to find the corresponding phase dynamics, we need to extend the definition of phase to the vicinity of limit-cycle because the external forcing may perturb the original limit-cycle. We define the concept of isochron $\chi(\boldsymbol{x})$ as the level set of $\theta(\boldsymbol{x})$, i.e. [127]

$$\chi(\boldsymbol{x}_0)=\big\{\boldsymbol{y}:\lim_{t\to\infty}|\boldsymbol{x}(t;\boldsymbol{x}_0)-\boldsymbol{x}(t;\boldsymbol{y})|=0\big\},\quad\forall\boldsymbol{x}_0\in\Gamma.$$

Here, we use $\boldsymbol{x}(t;\boldsymbol{x}_0)$ to represent the solution initiated at time 0 from $\boldsymbol{x}_0$. The strength of control $\boldsymbol{u}$ is required to be weak to keep the trajectory in the vicinity of Γ, which is consistent with the clinical treatment because the patient should not be stimulated strongly [7].

The evolution of phase is deduced from the law of chain derivative as

$$\dot{\theta}=\frac{\partial\theta}{\partial\boldsymbol{x}}\cdot\big(\boldsymbol{F}(\boldsymbol{x})+\boldsymbol{u}(\boldsymbol{x},t)\big).\tag{3.2}$$

A basic assumption in phase reduction theory is that the natural oscillation of the uncontrolled system possesses constant frequency, i.e. $(\partial\theta/\partial\boldsymbol{x})\cdot\boldsymbol{F}(\boldsymbol{x})=w$. Since the limit-cycle Γ is stable, we evaluate the dynamics on Γ to leading order as follows:

$$\dot{\theta}=w+\left.\frac{\partial\theta}{\partial\boldsymbol{x}}\right|_{\boldsymbol{x}^\gamma(\theta)}\cdot\boldsymbol{u}(t)\triangleq w+\boldsymbol{Z}(\theta)\cdot\boldsymbol{u}\big(\boldsymbol{x}^\gamma(\theta),t\big).\tag{3.3}$$

Here, $\boldsymbol{Z}(\theta)$ denotes the gradient of phase θ evaluated on the limit-cycle and is commonly referred to as the phase response curve (PRC) [23,72,77]. The PRC determine the reaction mechanism of the self-dynamics to the external forcing, which varies from different types of neuronal oscillators. However, analytical formulation of PRCs is lacking for most limit-cycle systems due to the irregular shape of the limit-cycle. In the context of neuronal oscillations, PRCs are further classified into two typical types: A Type I mode with as purely positive function values of PRC, and a Type II mode with PRC having negative parts [23]. Recent studies reveal a counter-intuitive phenomenon that the type of PRC may change due to the modulation of bioelectricity current and chemical media such as choline [25,37,116,130], instead of keeping a static PRC type. Our framework can take this PRC type transition into consideration by treating the external modulation as a change to the self-dynamics $\boldsymbol{F}(\boldsymbol{x})$. Specifically, consider $\boldsymbol{F}_0(\boldsymbol{x})$ and $\boldsymbol{F}_1(\boldsymbol{x})$ as the self-dynamics of the neuronal oscillation before and after the neuronal modulation, respectively. The changes of the self-dynamics lead to the changes of the periodic solution from which the phase variable $\boldsymbol{\theta}_{0,1}$ and phase frequency $w_{0,1}$ are extracted, and hence lead to the changes of the gradient of the phase functions $\boldsymbol{Z}_0(\boldsymbol{\theta}_0)$ and $\boldsymbol{Z}_1(\boldsymbol{\theta}_1)$. If the functions $\boldsymbol{Z}_0$ and $\boldsymbol{Z}_1$ belong to the Type I and the Type II PRCs, respectively, then we obtain an explanation of the PRC transition from the perspective of mathematical model.

To quantitatively identify the property of PRCs, we employ the following direct method that is extensively employed to find the PRCs [34,77]. We note that

$$\begin{aligned}
&\frac{\partial\theta}{\partial\boldsymbol{x}}=\left(\frac{\partial\theta}{\partial x_1},\dots,\frac{\partial\theta}{\partial x_d}\right)^{\intercal},\\
&\frac{\partial\theta}{\partial x_i}=\lim_{\varepsilon\to 0}\frac{\theta(\boldsymbol{x}+\varepsilon e_i)-\theta(\boldsymbol{x})}{\varepsilon}, \qquad i=1,\dots,d,\\
&\boldsymbol{x}=(x_1,\dots,x_d)^{\intercal}, \quad e_i=(0,\dots,\underbrace{1}_{i\text{-}th},\dots,0)^{\intercal}, \quad i=1,\dots,d.
\end{aligned} \tag{3.4}$$

Therefore, by quantifying the change of the phase resulting from the perturbation $\boldsymbol{x}\to\boldsymbol{x}+\varepsilon e_i$ for sufficient weak ε, we obtain the approximate PRC along the direction e_i as

$$\frac{\partial\theta}{\partial x_i}\approx\frac{\theta(\boldsymbol{x}+\varepsilon e_i)-\theta(\boldsymbol{x})}{\varepsilon}\triangleq\frac{\Delta_{\boldsymbol{x},\varepsilon}\theta}{\varepsilon}, \quad \boldsymbol{x}=\boldsymbol{x}^{\gamma}(\theta_0). \tag{3.5}$$

Since the phase motion has constant frequency and the limit-cycle is stable, the $\Delta_{\boldsymbol{x},\varepsilon}$ may be measured as the phase gap between $\boldsymbol{x}(t;\boldsymbol{x})$ and $\boldsymbol{x}(t;\boldsymbol{x}+\varepsilon e_i)$ for large t such that the perturbed trajectory collapse to the limit-cycle. For neuronal oscillations, the timing of a neural action potential generally corresponds to $\theta=0$. Then, $\Delta_{\boldsymbol{x}^{\gamma}(0),\varepsilon}$ can simply be inferred by measuring deviations from the expected timing between spikes and scaling the deviations. Similarly, the PRC at other phase can be measured by repeating the aforementioned procedure initiated from timing shifting after spike. For other general dynamical systems, more sophisticated methods are developed to obtain the PRCs, including solving the partial differential equations in adjoint method [24], processing the electroencephalogram (EEG) recordings with low signal-to-noise [110], and estimating the phase of a population of phase-locked [95] or phase-unlocked [55] oscillators from experimental data. For the completeness, we summarize the general formalism of phase reduction under coupled control as the end of this section, we also illustrate the workflow of phase reduction in Fig. 4(a).

Definition 3.1 (Phase Reduction)**.** *Consider the networked dynamics with N nodes as*

$$\dot{\boldsymbol{x}}_i=\boldsymbol{F}(\boldsymbol{x})+\sum_{j=1}^{N}A_{ij}\boldsymbol{H}(\boldsymbol{x}_i,\boldsymbol{x}_j), \quad \boldsymbol{x}\in\mathbb{R}^d, \tag{3.6}$$

here $\boldsymbol{A}=(A_{ij})$ is the network structure, $\boldsymbol{F}$ and $\boldsymbol{H}$ are the self dynamics of each node possessing a stable limit-cycle Γ and the interaction term between nodes, respectively. In phase reduction, we aim at finding the phase function $\theta=\theta(\boldsymbol{x})$ such that the corresponding phase dynamics takes the following closed-form formula:

$$\dot{\theta}_i=w+\sum_{j=1}^{N}A_{ij}\Gamma(\theta_i,\theta_j), \tag{3.7}$$

where w is the natural frequency of the self-dynamics, $\Gamma(\theta_i,\theta_j)$ is the interaction between nodes i,j depends only on their phases. The core idea in achieving the phase reduction is to find the PRC $\boldsymbol{Z}(\theta)=\partial\theta/\partial\boldsymbol{x}\big|_{\boldsymbol{x}^{\gamma}(\theta)}$. In phase reduction settings, the network structure is generally set as $A_{ij}=K/N$, where K represents the strength of coupling.

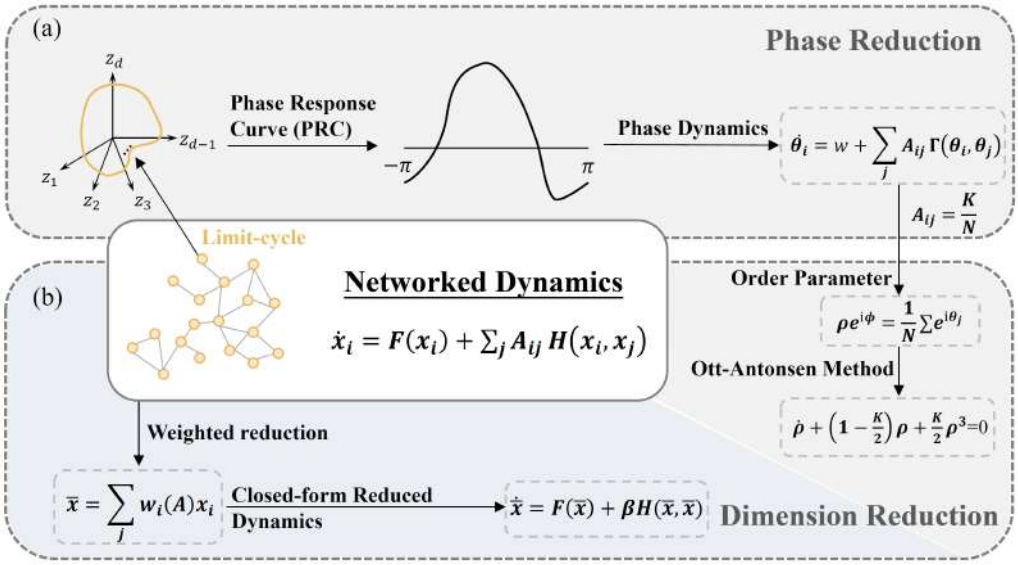

Figure 4: Illustration of the phase reduction and dimension reduction. (a) Phase reduction method reduces the d-dimensional limit-cycle oscillator to a closed-form scalar phase dynamics for each node. (b) Dimension reduction includes two approaches: The first is the Ott-Antonsen method that reduces the coupled phase dynamics of N nodes to closed-form dynamics of one scalar order parameter, and the second is Gao's method that reduces the coupled d-dimensional dynamics of N nodes $\boldsymbol{x}_i$ to a closed form d-dimensional dynamics of $\bar{\boldsymbol{x}}$, which is the weighted sum of $\boldsymbol{x}_i$.

Using the aforementioned phase reduction method, we further elaborate on the term "deciphering deep brain stimulation" used in the title of this article. We observe that the mechanism underlying the abnormal synchrony of neuron cells, which is relevant to the DBS field, lies in the phase response function of neuronal oscillators. Consequently, once the PRC of the relevant neuronal oscillators is uncovered, such as the Type I and the Type II PRCs, analyzing the onset of synchrony from the reduced phase dynamics of the neuronal cell population becomes feasible. Then, researchers are able to design treatments aiming at desynchronization of the abnormal synchrony, based on the insights gained from the reduced phase dynamics.

3.2 Dimension reduction

The aforementioned phase reduction method simplifies the dN-dimensional coupled oscillatory with d-dimensional self-dynamics and N oscillators to N-dimensional phase dynamics. To further reduce the complexity of the system, we introduce the dimension reduction methods, which simplify the N-dimensional phase dynamics to lower dimensional dynamics with effective dimension $n \ll N$ or even $n=1$. We begin with the classical Ott-Antonsen method, which plays a pivotal role in finding the low-dimensional behavior of the large dynamics [80]. For the collective neuronal oscillators inter-playing as the

Kuramoto model, the phase dynamics is described as

$$\dot{\theta}_i = w_i + \frac{K}{N}\sum_{j=1}^{N}\sin(\theta_j-\theta_i), \tag{3.8}$$

where each natural frequency $\{w_i, i=1,\dots,N\}$ is sampled from a given distribution $g(w)$. The coupling term in the left-hand side of Eq. (3.8) is related to the order parameter $r=(1/N)\sum_{j=1}^{N}\mathrm{e}^{\mathrm{i}\theta_j}$ as follows:

$$\frac{K}{N}\sum_{j=1}^{N}\sin(\theta_j-\theta_i)=\frac{K}{N}\sum_{j=1}^{N}\mathrm{Im}(\mathrm{e}^{\theta_j-\theta_i})=K\mathrm{Im}(r\mathrm{e}^{-\mathrm{i}\theta_i})=\frac{K}{2\mathrm{i}}\left(r\mathrm{e}^{-\mathrm{i}\theta_i}-r^*\mathrm{e}^{\mathrm{i}\theta_i}\right). \tag{3.9}$$

By substituting Eq. (3.9) into Eq. (3.8) and using the Liouville equation [53], we obtain the continuity equation for distribution of the phase $f(\theta,w,t)$ as

$$\frac{\partial f}{\partial t}+\frac{\partial}{\partial\theta}\left\{f\left[w+\frac{K}{2\mathrm{i}}\left(r\mathrm{e}^{-\mathrm{i}\theta}-r^*\mathrm{e}^{\mathrm{i}\theta}\right)\right]\right\}=0 \tag{3.10}$$

with the constraint

$$\int_0^{2\pi} f(\theta,w,t)\mathrm{d}\theta = g(w). \tag{3.11}$$

The following relation holds true in the limit of $N\to\infty$ from the law of large number [94],

$$r(t)=\int_0^{2\pi}\int_{-\infty}^{\infty}\mathrm{e}^{\mathrm{i}\theta}f(\theta,w,t)\mathrm{d}w\mathrm{d}\theta. \tag{3.12}$$

We consider the series expansion of f in interval $[0,2\pi]$ as

$$f=\sum_{k\in\mathbb{Z}}a_k\mathrm{e}^{\mathrm{i}k\theta},\quad a_k=\frac{1}{2\pi}\int_0^{2\pi}f\mathrm{e}^{-\mathrm{i}k\theta}\mathrm{d}\theta. \tag{3.13}$$

According to Eq. (3.11), we have $a_0=g(w)/(2\pi)$, leading to the equivalent formulation of f as

$$f=\frac{g(w)}{2\pi}\left[1+\sum_{k\neq 1}b_k\mathrm{e}^{\mathrm{i}k\theta}\right],\quad b_k=\frac{1}{g(w)}a_k. \tag{3.14}$$

Next, we restrict the expansion to a special case with $b_k=b_1^k$ and $k>0$. By substituting Eq. (3.13) into Eq. (3.10) and aligning the coefficients of the term $\mathrm{e}^{\mathrm{i}\theta}$, we obtain

$$\frac{\partial(b_1\mathrm{e}^{\mathrm{i}\theta})}{\partial t}+\frac{\partial}{\partial\theta}\left[wb_1\mathrm{e}^{\mathrm{i}\theta}+\frac{K}{2\mathrm{i}}\left(rb_1^2-r^*\right)\mathrm{e}^{\mathrm{i}\theta}\right]=0, \tag{3.15}$$

which further implies

$$\dot{b}_1+\frac{K}{2}\left(rb_1^2-r^*\right)+\mathrm{i}wb_1=0. \tag{3.16}$$

The relation between r and b_1 is deduced from Eqs. (3.12) and (3.14) as

$$r^*=\int_0^{2\pi}\int_{-\infty}^{\infty}\mathrm{e}^{-\mathrm{i}\theta}f(\theta,w,t)\mathrm{d}w\mathrm{d}\theta=\int_{-\infty}^{\infty}a_1\mathrm{d}w=\int_{-\infty}^{\infty}b_1g(w)\mathrm{d}w. \tag{3.17}$$

To proceed, we illustrate how to analyse the complex phase dynamics with the scalar dynamical system in Eq. (3.16). For example, the natural frequency of single cluster neuronal oscillators can be set as the unimodal Cauchy distribution

$$g(w)=\frac{h}{\pi}\frac{1}{(w-w_0)^2+h^2}. \tag{3.18}$$

Without loss of generality, we consider $w_0=0$ and $h=1$. By applying the residue theorem [115] to Eq. (3.17) at singular point $w_0-\mathrm{i}h$ of $g(w)$, we obtain

$$r^*=b_1(w_0-\mathrm{i}h,t)=b_1(-\mathrm{i}h,t). \tag{3.19}$$

Considering the polar coordinate representation $r=\rho\mathrm{e}^{\mathrm{i}\phi}$ and putting it into Eq. (3.15), we have

$$\dot{\rho}+\left(1-\frac{K}{2}\right)\rho+\frac{K}{2}\rho^3=0. \tag{3.20}$$

Here, $\rho=0$ is the equilibrium of the system representing the desynchronization state of the coupled oscillators, which is related to the normal state of brain. Therefore, by analyzing the stability of the equilibrium under patient specific parameters, we have the ability to identify and predict the symptoms of the patient from the theoretical perspective.

In addition to the reduction of single cluster of neuronal oscillators, more sophisticated dimension reduction methods have been cultivated in recent years. Thibeault *et al.* [121] consider phase dynamics with more general coupled terms instead of the Kuramoto model. Inspired by the Ott-Antonsen method, Wang *et al.* [125] propose the stability theory for dimension reduction method of multiple clusters of neuronal oscillators, which validates the feasibility of partial control in DBS. In this case, the effective dimension of reduced system equals to the number of clusters. Other methods have been developed that are applicable to oscillatory oscillators which are not described by the phase dynamics. Gao *et al.* [31] directly reduce the networked dynamics of oscillators as their weighted sum based on the structure of the network, the corresponding one-dimensional reduced system accurately reveals the tipping point of the original dynamics. Laurence *et al.* [58] improve Gao's method by replacing the weight vector as the solution of an optimization problem related to the eigendecomposition of the structure. Jiang *et al.* [50] take the cluster structure of the network into consideration, and proposes to apply Gao's method separately to each cluster of the network, leading to a more robust and effective reduced dynamics. We put the aforementioned Ott-Antonsen method and Gao's method for dimension reduction in Fig. 4(b). Similarly, we summarize the general formalism of dimension reduction as the end of this section.

Definition 3.2 (Dimension Reduction)**.** *Consider the networked dynamics in Eq.* (3.6)*, where, however, we do not require* $\boldsymbol{F}$ *has a stable limit-cycle. The aim of dimension reduction is to find a weight vector* $\boldsymbol{\alpha}=\boldsymbol{\alpha}(\boldsymbol{A})=(\alpha_1,\ldots,\alpha_n)^\intercal$*, a reduced weight* β*, and*

$$\dot{\bar{\boldsymbol{x}}}=\boldsymbol{F}(\bar{\boldsymbol{x}})+\beta\boldsymbol{H}(\bar{\boldsymbol{x}},\bar{\boldsymbol{x}}), \tag{3.21}$$

the closed-form dynamics of the weighted variable $\bar{\boldsymbol{x}}=\sum_i\alpha_i\boldsymbol{x}_i$ *such that the time trajectory of* $\bar{\boldsymbol{x}}(t)$ *in dynamics* (3.21) *approximate the weighted trajectory* $\sum_i\alpha_i\boldsymbol{x}_i(t)$ *in dynamics* (3.6) *in an optimal manner based on some prescribed measurement.*

The aforementioned dimensionality reduction methods pave the way to simplifying the complex networked dynamics of neuronal cells or biological oscillators. A direct application stemming from these reduction approaches is designing therapy strategies for patients by controlling the reduced dynamics. Generally, the networked dynamics exhibit high non-linearity, large spatial dimensions, and individual variability in each node, which pose difficulties for designing control policies. Through the phase reduction or dimension reduction method, the original complex system is reduced to a lower-dimensional system, thereby facilitating the design and analysis of control strategies for the system. Moving forward, we will introduce control theories in the next section that can be applied in such scenarios.

4 Control theories in DBS therapy

Controller synthesis often presents inherent difficulties, primarily due to the computational challenges arising from the high dimensionality of neuronal dynamics. To address this, dimensionality reduction techniques have been established, which allow us to construct a simplified system that accurately captures the basic features of the original higher-dimensional model, effectively mitigating the primary challenge. Consequently, the constructed simplified dynamics serve as an effective substitute for the original system, facilitating controller synthesis for complex dynamical systems. In the following sections, we delve into a few but essential control theories related to the DBS therapy.

We begin with a definition for the adaptive feedback control scheme.

Definition 4.1 (Adaptive Feedback Control)**.** *Consider a controlled system*

$$\dot{\boldsymbol{x}}=\boldsymbol{f}\big(\boldsymbol{x},\Theta(t),\boldsymbol{u}(t)\big), \tag{4.1}$$

where $\boldsymbol{x}(t)$ *is the state variable,* $\Theta(t)$ *is some unknown parameter or disturbances (may be high-dimensional, time-varying, and unbounded), and* $\boldsymbol{u}(t)$ *is the controller to be designed. If the controller* $\boldsymbol{u}(t)$ *does not depend on* $\Theta(t)$ *but only depends on the state* $\boldsymbol{x}(s)$ *for* $s\in[0,t]$*, the controller is said to be an adaptive feedback controller.*

Various mathematical models have been developed to explore the effectiveness of the DBS techniques for addressing synchronization-induced mental disorders. The DBS

techniques aim at eliminating synchronization in oscillatory neurons through the implementation of appropriate control scheme, broadly categorized into open-loop control [91] and closed-loop control (see Fig. 5(a)). It is widely acknowledged that, while open-loop control strategies exhibit limited robustness and consume considerable energy, closed-loop control approaches offer superior sustainability, robustness, and energy efficiency. Numerous feedback schemes have been validated as effective methods to achieve synchronization elimination in coupled neuronal networks [5,13,65,73,85–88,91,92,100,101]. Nevertheless, while the phenomenon of synchronization is destroyed, the signal waveform is also disrupted, thereby affecting the effective transmission of information within the neurons themselves [118]. Notably, adaptive control schemes have emerged in the previous studies [132,134], wherein the coupling gains dynamically adjust and optimize the values through system's evolution, thereby preserving the original waveform of the signal effectively.

4.1 Adaptive feedback control scheme

Modeling of the DBS treatment techniques has primarily focused on applying adaptive control to the dynamics of all nodes within the system [111,132–134], aiming to achieve desynchronization [12]. However, considering the clinical context where the DBS interventions are typically localized to specific brain regions, there arises a pertinent question regarding the implications of controlling only a subset of nodes on the dynamics of the entire system. In [125], they postulate the existence of two distinct clusters of neurons within this system (see Fig. 5(b)). Specifically, one of these clusters is dedicated to representing the target region, which is modulated through the application of DBS. Concur-

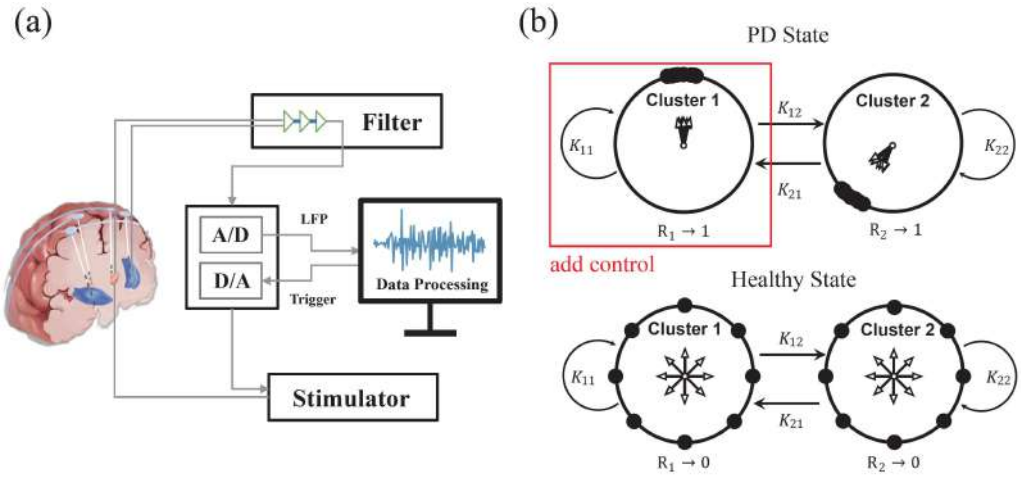

Figure 5: (a) A schematic of the closed-loop DBS strategy. (b) Applying control to only one cluster within the two-cluster systems facilitates the transition of the entire system from the PD state (upper panel) back to the healthy state (lower panel).

rently, the other cluster is sparsely connected to the target region and is thought to serve a distinct functional role within the larger network.

4.1.1 Adaptive scheme design for Eq. (2.18)

Initially, we add a feedback delay control on Eq. (2.18), which yields the system

$$\dot{z_j}=\left(\mathrm{i}w_j+1-|z_j|^2\right)z_j+KZ+L(t)Z_\tau,\quad j=1,2,\ldots,N, \tag{4.2}$$

where τ is the delay constant,

$$Z(t)=\frac{1}{N_1}\sum_{k=1}^{N_1}z_k(t),\quad Z_\tau=Z(t-\tau)$$

represents the feedback delay. $L(t)$ denotes a time-altered, complex-valued adaptive coupling strength. Using the transformation $z_j=\rho_j\mathrm{e}^{\mathrm{i}\theta_j}$ and letting $\rho_j\to 1$, we have the phase dynamics

$$\dot{\theta}_j=w_j+\mathrm{Im}\{[Kr+L(t)r(t-\tau)]\mathrm{e}^{-\mathrm{i}\theta_j}\}. \tag{4.3}$$

Let $L=|L|\mathrm{e}^{\mathrm{i}\gamma}$ where $L=C+\mathrm{i}S$. Hence, $C=|L|\cos\gamma$ and $S=|L|\sin\gamma$ with $\gamma\in(-\pi,\pi]$, which further yields

$$\dot{\theta}_j=w_j+\frac{K}{N}\sum_{i=1}^{N}\sin(\theta_i-\theta_j)+\frac{C}{N}\sum_{i=1}^{N}\sin[\theta_i(t-\tau)-\theta_j]+\frac{S}{N}\sum_{i=1}^{N}\cos[\theta_i(t-\tau)-\theta_j]. \tag{4.4}$$

To formulate an adaptive technique for the coupled Kuramoto system, we define the energy function as

$$Q\triangleq Q_\tau(t)=|r_1(t-\tau)|^2=|r_{1,\tau}|^2=r_{1,\tau}r_{1,\tau}^*$$

whenever $\tau>0$. In this pursuit, the information exclusively from the first cluster in a two-cluster system is utilized. Thus, the synchronized state and the desynchronized state correspond to $|r_1(t)|\equiv 1$ and $r_1(t)\equiv 0$, respectively. The steady states are typically exist at the minimal or/and the maximal values of Q. Leveraging the steepest descent method (SDM), setting $r_1(t)\equiv 0$ as the target state, and ascertaining the minimum of $Q_\tau(t)$, the dynamics governing the real and imaginary components of the adaptive scheme L are designed as follows:

$$\dot{C}=-\eta_1\cdot\partial_C\dot{Q}\cdot H(|r_{1,\tau}|-\epsilon),\quad \dot{S}=-\eta_2\cdot\partial_S\dot{Q}\cdot H(|r_{1,\tau}|-\epsilon), \tag{4.5}$$

where $\eta_{1,2},\epsilon>0$ are adjustable control parameters, and H is the standard Heaviside step function. The explicit form of the energy can be computed as

$$Q=|r_1(t-\tau)|^2=\left|\frac{1}{N_1}\sum_{j=1}^{N_1}\mathrm{e}^{\mathrm{i}\theta_j(t-\tau)}\right|^2.$$

The energy without delay is defined as $Q_0(t)$, and then

$$\dot{Q}_0(t)=\dot{r}_1(t)r_1^*(t)+\text{c.c.}=2\text{Re}\{\dot{r}_1(t)r_1^*(t)\}, \tag{4.6}$$

where c.c. represents the complex conjugate of the preceding formula, and

$$\begin{aligned}\dot{r}_1(t)&=\frac{1}{N_1}\sum_{j=1}^{N_1}\text{i}e^{\text{i}\theta_j}\dot{\theta}_j\\&=\frac{1}{N_1}\sum_{j=1}^{N_1}\text{i}e^{\text{i}\theta_j}\left\{w_j+\frac{1}{2\text{i}}[Kr+Lr(t-\tau)]e^{-\text{i}\theta_j}-\frac{1}{2\text{i}}[Kr^*+Lr^*(t-\tau)]e^{\text{i}\theta_j}\right\}\\&\triangleq\frac{L}{2}r_1(t-\tau)-\frac{L}{2}r_1^*(t-\tau)s_1(t)+g(\theta,K,N).\end{aligned}$$

Here $s_1(t)\triangleq(1/N_1)\sum_{j=1}^{N_1}e^{2\text{i}\theta_j}$ and $g(\theta,K,N)$ is generated by θ,K, and N. By $L=C+\text{i}S$, the control can be written as

$$\begin{aligned}\partial_C\dot{Q}_0(t)&=\text{Re}\{r_1(t-\tau)r_1^*(t)-r_1^*(t-\tau)r_1^*(t)s_1(t)\},\\\partial_S\dot{Q}_0(t)&=-\text{Im}\{r_1(t-\tau)r_1^*(t)-r_1^*(t-\tau)r_1^*(t)s_1(t)\}.\end{aligned} \tag{4.7}$$

Then, by taking $t=t-\tau$ and the adaptive control scheme can be rewritten as

$$\begin{aligned}\dot{C}&=-\eta_1\text{Re}\{[r_{1,2\tau}r_{1,\tau}^*-r_{1,2\tau}^*r_{1,\tau}^*s_{1,\tau}]\}H(|r_{1,\tau}|-\epsilon),\\\dot{S}&=\eta_2\text{Im}\{[r_{1,2\tau}r_{\tau}^*-r_{1,2\tau}^*r_{1,\tau}^*s_{1,\tau}]\}H(|r_{1,\tau}|-\epsilon).\end{aligned} \tag{4.8}$$

When consider the coupled Stuart-Landau equations, the complex-valued coupling gain dynamically obeys

$$\begin{aligned}\dot{C}&=-2\eta_1\text{Re}\{Z_{2\tau}Z_{\tau}^*\}H(|Z_{\tau}|-\epsilon),\\\dot{S}&=2\eta_2\text{Im}\{Z_{2\tau}Z_{\tau}^*\}H(|Z_{\tau}|-\epsilon).\end{aligned} \tag{4.9}$$

4.1.2 Feasible parameter regions

In order to analytically illustrate the feasibility of the adaptive techniques proposed above, we set $L(t)\equiv L=C+\text{i}S$ as a constant number in (4.4), so that we need to locate the parameter region of L in the complex plane for eliminating synchronization for (4.4). To this end, using the Ott-Antonsen ansatz leads to that

$$\dot{\alpha}=-\text{i}w\alpha-\frac{K}{2}(r\alpha^2-r^*)-\frac{L}{2}[r(t-\tau)\alpha^2-r(t-\tau)^*], \tag{4.10}$$

where the order parameter is

$$r^*=\int_{-\infty}^{+\infty}\alpha(w,t)g(w)\text{d}w. \tag{4.11}$$

In this section, we consider a special case of the natural frequency distribution as

$$g(w)=\frac{\sqrt{2}}{\pi}\cdot\frac{1}{w^4+1}, \tag{4.12}$$

which has not been discussed yet in the literature.

Firstly, we try to obtain an analytical expression for r^*. As discussed in [80], the function $\alpha(w,t)$ can be analytically extended to the lower half complex plane (see Fig. 6(a)), satisfying $|\alpha(w,t)|\leq 1$. Denote by $\Gamma_R \triangleq S_R \cup T_R$ the closed curve in the lower half complex plane, where

$$S_R \triangleq \{s \mid s: R\to -R\}, \quad T_R \triangleq \{Re^{i\theta} \mid \theta:\pi\to 2\pi\}.$$

Note that $g(w)$ has two poles, i.e. $w=e^{-\pi i/4}, e^{-3\pi i/4}$, in the lower-half complex plane. According to the residue theorem [115], we obtain

$$\int_{\Gamma_R} g(w)\alpha(w,t)dw = 2\pi i\left[\mathrm{Res}\left(g\alpha, e^{-\frac{\pi i}{4}}\right)+\mathrm{Res}\left(g\alpha, e^{-\frac{3\pi i}{4}}\right)\right]. \tag{4.13}$$

Here, $R>0$ is sufficiently large. $\mathrm{Res}(\cdot,\cdot)$ represents the residue for a given analytical function. By utilizing L'Hopital's rule, we obtain

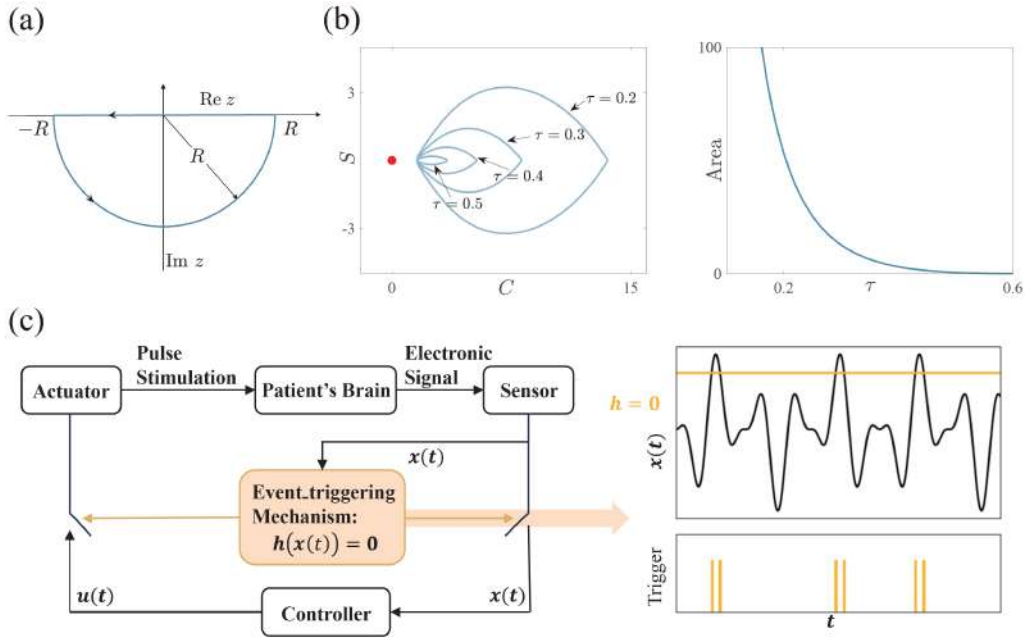

Figure 6: (a) The contour Γ_R used in Eq. (4.13). (b) When $K=3$, the feasible stability region shrinks as τ increases. (c) The event-based DBS gives pulse stimulation to patient once the monitored brain signal $\boldsymbol{x}(t)$ satisfies the triggering condition $h(\boldsymbol{x}(t))=0$.

$$\begin{aligned}\mathrm{Res}\big(g\alpha,\mathrm{e}^{-\frac{\pi\mathrm{i}}{4}}\big)&=\lim_{w\to\mathrm{e}^{-\pi\mathrm{i}/4}}\big(w-\mathrm{e}^{-\frac{\pi\mathrm{i}}{4}}\big)\cdot\frac{\sqrt{2}}{\pi}\cdot\frac{1}{w^4+1}\alpha(w,t)\\&=\frac{\sqrt{2}}{\pi}\alpha\big(\mathrm{e}^{-\frac{\pi\mathrm{i}}{4}},t\big)\cdot\frac{1}{4\cdot\mathrm{e}^{-3\pi\mathrm{i}/4}},\end{aligned}\tag{4.14}$$

$$\begin{aligned}\mathrm{Res}\big(g\alpha,\mathrm{e}^{-\frac{3\pi\mathrm{i}}{4}}\big)&=\lim_{w\to\mathrm{e}^{-\frac{3\pi\mathrm{i}}{4}}}\big(w-\mathrm{e}^{-\frac{3\pi\mathrm{i}}{4}}\big)\cdot\frac{\sqrt{2}}{\pi}\cdot\frac{1}{w^4+1}\alpha(w,t)\\&=\frac{\sqrt{2}}{\pi}\alpha\big(\mathrm{e}^{-\frac{3\pi\mathrm{i}}{4}},t\big)\cdot\frac{1}{4\cdot\mathrm{e}^{-9\pi i/4}}\\&=\frac{\sqrt{2}}{\pi}\alpha\big(\mathrm{e}^{-\frac{3\pi\mathrm{i}}{4}},t\big)\cdot\frac{1}{4\cdot\mathrm{e}^{-\pi\mathrm{i}/4}}.\end{aligned}\tag{4.15}$$

Furthermore, we have the estimations as

$$\begin{aligned}\left|\int_{T_R}g(w)\alpha(w,t)\mathrm{d}w\right|&=\left|\int_{T_R}\frac{\sqrt{2}}{\pi}\cdot\frac{1}{w^4+1}\alpha(w,t)\mathrm{d}w\right|\\&=\left|\int_{\pi}^{2\pi}\frac{\sqrt{2}}{\pi}\cdot\frac{\mathrm{i}R\mathrm{e}^{\mathrm{i}\theta}}{R^4\mathrm{e}^{4\mathrm{i}\theta}+1}\alpha(R\mathrm{e}^{\mathrm{i}\theta},t)\mathrm{d}\theta\right|\\&\le\int_{\pi}^{2\pi}\frac{\sqrt{2}}{\pi}\left|\frac{\mathrm{i}R\mathrm{e}^{\mathrm{i}\theta}}{R^4\mathrm{e}^{4\mathrm{i}\theta}+1}\right||\alpha(R\mathrm{e}^{\mathrm{i}\theta},t)|\mathrm{d}\theta\\&\le\sqrt{2}\frac{R}{R^4-1}\ \to\ 0\quad(R\ \to\ +\infty).\end{aligned}\tag{4.16}$$

Letting $R\to+\infty$ of both sides of Eq. (4.13) yields

$$r^*=-2\pi\mathrm{i}\cdot\left[\frac{\sqrt{2}}{\pi}\alpha\big(\mathrm{e}^{-\frac{\pi\mathrm{i}}{4}},t\big)\cdot\frac{1}{4\cdot\mathrm{e}^{-3\pi\mathrm{i}/4}}+\frac{\sqrt{2}}{\pi}\cdot\alpha\big(\mathrm{e}^{-\frac{3\pi\mathrm{i}}{4}},t\big)\cdot\frac{1}{4\cdot\mathrm{e}^{-\pi\mathrm{i}/4}}\right].\tag{4.17}$$

Substituting $w=\mathrm{e}^{-\pi\mathrm{i}/4},\mathrm{e}^{-3\pi\mathrm{i}/4}$ into Eq. (4.10) yields

$$\begin{cases}\dot{\alpha_1}=\dfrac{\sqrt{2}}{2}(-\mathrm{i}-1)\alpha_1-\dfrac{K}{2}\big(r\alpha_1^2-r^*\big)-\dfrac{L}{2}\big[r(t-\tau)\alpha_1^2-r(t-\tau)^*\big],\\[2mm]\dot{\alpha_2}=\dfrac{\sqrt{2}}{2}(\mathrm{i}-1)\alpha_2-\dfrac{K}{2}\big(r\alpha_2^2-r^*\big)-\dfrac{L}{2}\big[r(t-\tau)\alpha_2^2-r(t-\tau)^*\big],\\[2mm]r^*=\dfrac{\mathrm{i}+1}{2}\alpha_1-\dfrac{\mathrm{i}-1}{2}\alpha_2,\end{cases}\tag{4.18}$$

where $\alpha_1=\alpha(\mathrm{e}^{-\pi\mathrm{i}/4},t)$ and $\alpha_2=\alpha(\mathrm{e}^{-3\pi\mathrm{i}/4},t)$. We intend to find the parameter region of L for ensuring stability of $\alpha_{1,2}=0$ of Eq. (4.18) (i.e. achieving an elimination of the

synchronization). A linearization of Eq. (4.18) at $\alpha_1=\alpha_2=0$ gives $\dot{\boldsymbol{x}}=\boldsymbol{H}\boldsymbol{x}+\boldsymbol{G}\boldsymbol{x}(t-\tau)$, where $\boldsymbol{x}=[\alpha_1,\alpha_2]^\intercal$,

$$H=\begin{bmatrix}\frac{\sqrt{2}}{2}(-\mathrm{i}-1)+\frac{K}{4}(\mathrm{i}+1) & -\frac{K}{4}(\mathrm{i}-1)\\ \frac{K}{4}(\mathrm{i}+1) & \frac{\sqrt{2}}{2}(\mathrm{i}-1)-\frac{K}{4}(\mathrm{i}-1)\end{bmatrix},$$
$$G=\begin{bmatrix}\frac{L}{4}(\mathrm{i}+1) & -\frac{L}{4}(\mathrm{i}-1)\\ \frac{L}{4}(\mathrm{i}+1) & -\frac{L}{4}(\mathrm{i}-1)\end{bmatrix}.$$

Hence, the characteristic equation $\det[\lambda I-H-\mathrm{e}^{-\lambda\tau}G]=0$ is computed as

$$\begin{aligned}&\left[\lambda-\frac{\sqrt{2}}{2}(-\mathrm{i}-1)-\frac{K}{4}(\mathrm{i}+1)-\frac{L}{4}\mathrm{e}^{-\lambda\tau}(\mathrm{i}+1)\right]\left[\lambda-\frac{\sqrt{2}}{2}(\mathrm{i}-1)+\frac{K}{4}(\mathrm{i}-1)+\frac{L}{4}\mathrm{e}^{-\lambda\tau}(\mathrm{i}-1)\right]\\&\quad-\left(-\frac{K}{4}(\mathrm{i}-1)-\frac{L}{4}\mathrm{e}^{-\lambda\tau}(\mathrm{i}-1)\right)\left(\frac{K}{4}(\mathrm{i}+1)+\frac{L}{4}\mathrm{e}^{-\lambda\tau}(\mathrm{i}+1)\right)=0\end{aligned}$$

Using the geometric approach developed in [134, Appendix B], we obtain the feasible stability region for L in the complex plane. As seen in Fig. 6(b), the stability region shrinks as τ increases. This suggests that the time delay plays a negative role in forming a stability region in the complex plane of L.

4.2 Event-triggered control scheme

The aforementioned feedback control scheme requires continuously monitoring the potential signal of patients, such as EEG signal, and updating the control signal, which may accumulate too much energy to patient. To alleviate the pressure exerted on the patient by the continuous application of control signal, event-based methods have been employed. Compared to the feedback control which updates the control signal at a series of predefined explicit times, event-triggered control (refer to Fig. 6(c)) updates the control signal at the instants when the current measurements violate a predefined triggering condition, thereby triggering a state-dependent event [45].

According to the specific observable variables in neuromodulation systems based on electrical stimulation, different event mechanisms are set to modulate the duration of control stimulation to the patient. In [106], local field potential (LFP) is selected as the observable variable and the electrical stimulation applied to the patient is triggered once the LFP crosses a certain threshold. Specifically, the threshold on the LFP amplitude is set at -3 RMS, the LFP is dynamically computed with a history of 30 seconds. The 100 milliseconds post-stimulation history is excluded from the computation to avoid contamination by the stimulation artifact. In [43, 62–64, 68, 84, 122], the adaptive deep brain stimulation (ADBS) mechanism is considered, in which the beta band LFP is monitored,

and the threshold for triggering the stimulation was set manually so that the DBS would be switched on for about 50% of the time when the patient was at rest.

For completeness, below we give the mathematical description of the event triggered control scheme in DBS tasks.

Definition 4.2 (Event-Triggered Control)**.** *Consider the controlled system as*

$$\dot{\boldsymbol{x}} = \boldsymbol{f}\big(\boldsymbol{x}, \boldsymbol{u}(t)\big), \tag{4.19}$$

where the event-triggered implementation of the feedback controller is defined as $\boldsymbol{u}(t) = \boldsymbol{K}(\boldsymbol{x}(t_k))$, $t_k \le t < t_{k+1}$, *while the triggering time is decided by*

$$t_{k+1} = \inf\big\{t > t_k : h\big(\boldsymbol{x}(t)\big) = 0\big\}$$

for some predefined event function h.

Specifically, in the aforementioned examples, the state $\boldsymbol{x}$ is set as the LFP signal, the event function h is set as the difference of $\boldsymbol{x}$ and the predefined threshold.

5 AI-driven control

We note that the exact mechanisms of DBS are still a matter of debate [21, 35, 51], and therefore finding effective DBS policies requiring the control policies for different kinds of dynamical systems. Due to the high dimension and non-linearity property of brain neurons, the neuronal dynamics are generally coupled with complicated structure and complex dynamics. Therefore, traditional control methods based on delicate design of the control formulation fail to handle such elaborate tasks. Since the universal approximation theory of neural networks was proposed by [16], AI-driven control methods have been developed to circumvent the problems incurred by highly complex systems in the interdisciplinary fields of medical treatment, control theory and biomathematics. We review two major types of control policies in DBS: optimal control and stabilization control, as illustrated in Fig. 7. In our review, the methods introduced in optimal control belong to the data-driven settings in which we only have the measurement data of the brain signals, while the stabilization control belong to the model-driven cases where the mathematical models of neuronal dynamics are known. As both of the control problems have been studied extensively using the traditional techniques [60, 120], recent advancements in machine learning pave a way to cultivate more efficient and practical control policies for them.

5.1 Optimal control

Suppression of the abnormal synchronous behavior of coupled neuronal dynamics has been widely accepted as the goal of the DBS. Since the suppression process corresponds

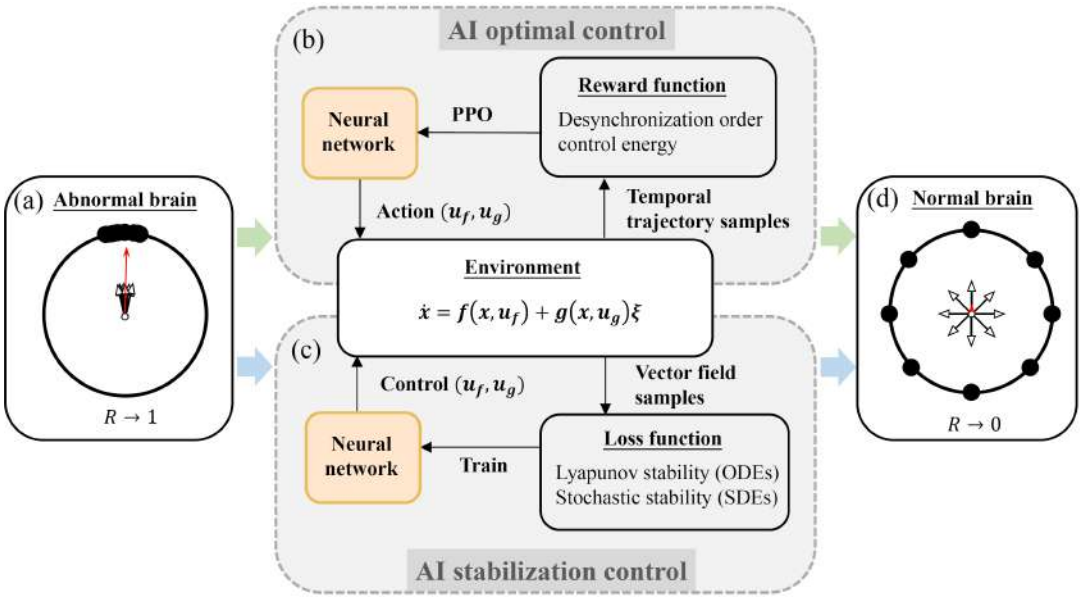

Figure 7: An illustration of the AI control methods for realizing the DBS. (a) The abnormal brain state corresponds to the synchronization of neuronal oscillators. To eliminate the synchronization, both the optimal control (b) and stabilization control (c) are considered to design the neural network based treating policy from the mathematical model of coupled neuronal system. (d) After control, the synchronization phenomenon is suppressed to achieve the normal brain state.

to control of a large network of interacting neurons, the target of the DBS can be naturally regarded as an optimal control problem that achieving the best performance while obeying the dynamics of neurons. In the optimal control setting, we have an objective functional depending on controlled trajectory and the controller that measures the performance of the control process. The task is to find the best controller that maximize the objective functional under specific constraints, e.g. the controlled state evolves along the controlled dynamics and the control value should not exceed a certain threshold. A general mathematical formulation of the optimal control problem is described as follows:

$$\begin{aligned} &\max_{\boldsymbol{u}_{0:T}} J(\boldsymbol{x}_0, \boldsymbol{u}_{0:T}) \triangleq \sum_{t=0}^{T} \gamma^t r\big(\boldsymbol{x}(t), \boldsymbol{u}(t)\big), \\ &\text{s.t.} \quad \boldsymbol{x}(t+1) = \boldsymbol{f}\big(\boldsymbol{x}(t), \boldsymbol{u}(t)\big), \\ &\boldsymbol{u}(t) \in \mathcal{U}(t), \end{aligned} \tag{5.1}$$

where r is the reward function depending on the controlled state $\boldsymbol{x}$ and the control value $\boldsymbol{u}$, γ is the discount factor, $\boldsymbol{f}$, dubbed as environment, defines the controlled dynamics, $\mathcal{U}(t)$ captures the constraint on the control value at time step t. In the last decades, many control methods are developed to handle such kind of problem under the DBS settings, including both online learning methods, e.g. model predictive control [38,61], and offline learning methods, e.g. model-based reinforcement learning (RL) [32]. Generally speak-

ing, online learning methods has the ability to find the optimal control value at specific time, while offline learning methods aim at finding the optimal control policy for a range of time and depends on the mathematical models of brain dynamics [105,129]. From the clinical treatment perspective, an ideal control policy should quickly response to the current state of patient. Nevertheless, the online learning control methods, incurring solving iterative optimization problem of high-dimensional neuronal system, have large computational complexity. Consequently, we focus on the offline learning methods that provide closed-form control function of the state.

Concretely, we consider the AI-based RL method in the DBS problem studied in [56]. The environment of the neuronal populations in the DBS task is selected as the globally coupled FHN oscillators

$$\begin{aligned} \dot{x}_i &= x_i - \frac{x_i^3}{3} - y_i + I_i + \varepsilon \frac{1}{N}\sum_{j=1}^{N} x_j + u(t), \\ \dot{y}_i &= 0.1(x_i - 0.8y_i + 0.7). \end{aligned} \tag{5.2}$$

Here, we consider the Euler iteration with temporal sampling rate δ of the continuous dynamics as the realization of the environment, and focus on the mean field observable variable $X=(1/N)\sum_{i=1}^{N} x_i$ and $Y=(1/N)\sum_{i=1}^{N} y_i$. For the sub-threshold coupling, these variables own a fixed point, approximately $X^*\approx -0.27$ and $Y^*\approx 0.55$. The difficulty in realizing the optimal control for this system arises from the fact that the fixed point to be stabilized is not in the origin and is priorly unknown. After we settle the environment, we pre-define the current state-action set at time step $t_n = n\Delta$ as $\{X_{t_{n-k+1}}, Y_{t_{n-k+1}}, u_{t_{n-k+1}}\}_{k=0}^{M-1}$, where $\Delta = l\delta$ for some integer $l>1$. This set is fed to the RL method to assess the reward in the last m time steps. To proceed, we define the control policy as

$$\begin{aligned} u(t) &= \sum_n A_n P_n(t), \quad A_{\min} \le A_n \le A_{\max}, \\ P_n(t) &= \begin{cases} 1, & t_n \le t \le t_n + \tau, \\ 0, & \text{otherwise}, \end{cases} \end{aligned} \tag{5.3}$$

in which $A_{\min}, A_{\max}$ are the constraints on the control value, and $0<\tau<\Delta$ are the predefined time constants. To identify the specific control value A_n given the current state X_{t_n}, we use the neural network to parameterize the policy $\pi_{\theta} = \mathbb{P}(X_{t_n}, A_n)$ such that the controller takes value A_n with probability $\mathbb{P}(X_{t_n}, A_n)$. Then, by applying the control policy to the environment and collect the obtained state-action set, we calculate the reward function as

$$\begin{aligned} r(t_n) &= -\left(X_{t_n} - \frac{1}{M}\sum_{k=1}^{M} X_{t_{n-k+1}}\right)^2 - 2\frac{1}{\Delta}\sum_{k=1}^{M} |u_{t_{n-k+1}}|, \\ J_{\pi} &= \mathbb{E}_{\pi}\left[\sum_{n=1}^{N} \gamma^n r(t_n)\right]. \end{aligned} \tag{5.4}$$

Finally, we use a proximal policy optimization (PPO) [108] method to update the parameters $\boldsymbol{\theta}$ of the neural network.

5.2 Stabilization control

The suppression of synchronous neuron system in the DBS is also related to the stabilization control by recasting the problem as stabilize the equilibrium representing the normal brain state [125]. According to the different brain models considered in the DBS settings, the specific stabilization control tasks take different formulations. Here, we review several representative stabilization control of DBS and summarize their drawbacks in realistic scenarios. Firstly, in [93], the DBS is regarded as an effective therapy for systematic treatment of symptoms of movement disorders such as essential tremor. To alleviate the patients' tremor behavior, researchers utilize an oscillator for representation of the overall brain and muscle dynamics of a tremor-oriented disease for the simplicity of tremor control. The tremor dynamics of the oscillator is described as follows:

$$\begin{aligned} \dot{x}_1 &= af(t,x_1) - w^2 x_2 + [u(t) - A], \\ \dot{x}_2 &= x_1 - bx_2, \\ y &= Cx_1, \end{aligned} \tag{5.5}$$

where x_1 and x_2 are the states of the oscillator, y represents the tremor, the parameters a and b represent the effects of nonlinear and stabilization terms, C and w are time-varying parameters representing the strength of amplitude and the angular frequency of the tremor, respectively, A is the nominal value of stimulation amplitude, f is the nonlinear term differing from different patients, and $u(t)$ is the control signal for amplitude of the stimulus signal. The target in this task is to stabilize the tremor y to zero. To achieve this task for general nonlinear function f, delicate feedback control and Lyapunov function are constructed for f to guarantee the stability of $y = 0$ based on the Lyapunov stability theory. Nevertheless, this method suffers from the cumbersome construction for different specific function f and the obtained controlled dynamics may not be stable facing the inevitable intrinsic noise in the tremor signal.

Secondly, the firing-rate model, which is inspired by the STN-GPe loop model originally proposed in [78], is extensively used to study the emergence of pathological beta oscillations observed in the parkinsonian basal ganglia [30]. Hence, researchers derive the self-tuning DBS control in this model as follows:

$$\begin{aligned} \tau_1 \dot{x}_1 &= -x_1 + S_1[c_{11}x_1(t-\delta_{11}) - c_{12}x_2(t-\delta_{12}) + b_1 u_1(t)], \\ \tau_2 \dot{x}_2 &= -x_2 + S_2[c_{21}x_1(t-\delta_{21}) - c_{22}x_2(t-\delta_{22}) - b_2 u_2(t)]. \end{aligned} \tag{5.6}$$

Here, x_1 and x_2 respectively represent the instantaneous firing activities of the STN and GPe, $\tau_1, \tau_2 > 0$ are time constants. The constant $c_{ij} \geq 0$ represents the synaptic connection strength from population j to population i and $\delta_{ij} \geq 0$ is a time delay that occurs due to finite velocity of axonal and synaptic transmission from population j to population i.

u_1 and u_2 represent the influence of cortical (into STN) and striatal (into GPe) inputs to the system, respectively, modulated by the synaptic weights $b_1 \geq 0$ and $b_2 \geq 0$. The activation functions S_1 and S_2 encode the response of the neuronal populations to their input. It was revealed that under the constant cortical and striatal inputs (u_1,u_2), the firing-rate model exists an equilibrium $\bar{\boldsymbol{x}}=(\bar{x}_1,\bar{x}_2)$ [82], subject to the corresponding variational equation of $\boldsymbol{x}\leftarrow\boldsymbol{x}-\bar{\boldsymbol{x}}$ and $\boldsymbol{u}\leftarrow\boldsymbol{u}-\bar{\boldsymbol{u}}$ under control $\mu(t)$ acting on STN satisfies the following dynamics:

$$\begin{aligned}\tau_1\dot{x}_1&=-x_1+S_1[c_{11}x_1(t-\delta_{11})-c_{12}x_2(t-\delta_{12})+\mu(t)],\\ \tau_2\dot{x}_2&=-x_2+S_2[c_{21}x_1(t-\delta_{21})-c_{22}x_2(t-\delta_{22})].\end{aligned}\tag{5.7}$$

Here, we shift the activation function $S_j, j=1,2$ subject to $S_j(0)=0$ for simplicity. The task now is to stabilize the system from the oscillation state to the equilibrium. Although it was shown that a proportional feedback acting only on STN is capable of achieving this stabilization task [39,82], the difficult of choosing suitable strength depending on specific form of activation function S_j and the cumbersome theoretical analysis for the stability certificate restrict the application of the proportional feedback.

Thirdly, since cluster synchronization underlies various functions in the brain, abnormal patterns of cluster synchronization are often associated with neurological disorders. Therefore, Yuzhen Qin *et al.* [89] regard DBS as a neurosurgical technique to treat several brain diseases through regulating neuronal cluster synchrony patterns. Specifically, consider the coupled neuronal oscillators governed by the following Kuramoto model:

$$\dot{\theta}_i=w_i+\sum_{j=1}^{N}a_{ij}\sin(\theta_j-\theta_i),\tag{5.8}$$

where the n oscillators are coupled on an undirected network with node set $\mathcal{V}=\{v_1,\ldots,v_n\}$ and weighted adjacency matrix $\boldsymbol{A}=\boldsymbol{A}^{\intercal}=(a_{ij})_{n\times n}$. The cluster synchronization manifold is defined as

$$\mathcal{M}=\{\theta_i=\theta_j,\ \forall i,j\in\mathcal{C}_k,\ k=1,\ldots,r\}\tag{5.9}$$

on partition of $\mathcal{V}:\mathcal{C}_i\cap\mathcal{C}_j=\emptyset, 1\leq i\neq j\leq r, \cup_{k=1}^{r}\mathcal{C}_k=\mathcal{V}$. To guarantee the normal function of brain with feasible regulation, the task here is to stabilize the coupled system to the cluster synchronization manifold $\mathcal{M}$ via fine tuning the adjacency matrix as follows:

$$\begin{aligned}\dot{\theta}_i&=w_i+\sum_{j=1}^{N}[a_{ij}+q(a_{ij})u_{ij}(t)]\sin(\theta_j-\theta_i),\\ q(a_{ij})&=\begin{cases}1, & a_{ij}>0,\\ 0, & \text{otherwise.}\end{cases}\end{aligned}\tag{5.10}$$

Here, $\boldsymbol{u}(t)=u_{ij}(t)$ is the corresponding control input representing the influence of the DBS to the axons and dendrites of nerve cells. In [89], the vibrational control theory is utilized to obtain the stability under specific periodic form controller $\boldsymbol{u}(t)$. Nonetheless, the open-loop control cannot provide the adaptive stability under prevalent perturbation and noise in brain system, and the specific control form is hard to achieve in practice.

Lastly, K. Wang *et al.* [80, 125] study the following low-dimensional behavior of networked controlled Kuramoto dynamics considered in Eq. (2.18) under Ott-Antonsen method

$$\dot{\alpha}+\frac{K}{2}(r\alpha^2-r^*)+\frac{L(t)}{2}\big(r(t-\tau)\alpha^2-r(t-\tau)^*\big)+\mathrm{i}w\alpha=0. \tag{5.11}$$

In this reduced dynamics, the zero solution of $\alpha=r^*$ corresponds to the desynchronization state in the original coupled system. Therefore, the aim is to design control strength $L(t)=L(\alpha(t))$ to stabilize the desynchronization equilibrium. Despite the fact that this method benefits from handling a scalar controlled dynamics instead of the high-dimensional networked dynamics, the use of Ott-Antonsen method restrict the controller in mean field control form $\boldsymbol{u}=L(t)Z$ in the original space.

All the mentioned examples illustrate how to recast designing the DBS strategies into stabilization control tasks. To finding the stabilization control policies, amounts of efficient control methods are proposed in the last several decades. For stabilizing linear or polynomial dynamical systems, the linear quadratic regulator (LQR) [54] and the sum-of-squares (SOS) polynomials through the semi-definite planning (SDP) [81] have been extensively developed using the standard Lyapunov stability theory. For more general and nonlinear dynamical systems, linearization technique around the equilibria is often utilized and thus the previous control policies are effective in the vicinity of the equilibria [107] but likely lose efficacy in the region far away from those states. However, all the previous methods are limited to specific scenarios, ensuing from the difficulty of analytically constructing specific control functions and stability certificate functions to ensure the stability of the controlled system. To address this issue, designing the stabilization controllers using neural networks (NNs) becomes one of the mainstream approaches in the interdisciplinary community of control and biomedicine [17, 69, 83, 124]. One of the representative methods is using NNs to construct the Lyapunov function and the control function simultaneously [11, 131]. In this way, the controller is applied with confidence because the NN-based Lyapunov function provides the stability certificate.

Specifically, we consider the general controlled system described by the following ordinary differential equations (ODEs):

$$\dot{\boldsymbol{x}}(t)=\boldsymbol{f}\big(\boldsymbol{x}(t),\boldsymbol{u}(\boldsymbol{x})\big)\triangleq\boldsymbol{f}_{\boldsymbol{u}}(\boldsymbol{x}),\quad \boldsymbol{x}(t)\in\mathbb{R}^d, \tag{5.12}$$

which represents a general form for reduced-order dynamical systems, such as Eq. (5.11). As we discussed in the last paragraph of Section 2.3.2, $\boldsymbol{x}\equiv\mathbf{0}$ signifies the desynchronization state. This further indicates that the unstable zero solution of the original system corresponds to an abnormal brain state. The aim of deep brain stimulation is to stabilize this unstable equilibrium using a non-invasive control input such that $\boldsymbol{u}(\mathbf{0})=\mathbf{0}$. In this review, we consider the classic Lyapunov stability for the controlled system.

Theorem 5.1 ([2], Lyapunov Stability)**.** *For the controlled system* (5.12)*, suppose there exists a continuously differentiable function $V:\mathcal{D}\to R$ that satisfies the following conditions:*

(i) $V(0)=0$,
(ii) $V(\boldsymbol{x})>0$ *for all* $\boldsymbol{x}\neq\boldsymbol{0}$,
(iii) $\mathcal{L}_{f_u}V\triangleq\nabla V(\boldsymbol{x})\cdot\boldsymbol{f}(\boldsymbol{x},\boldsymbol{u})<0$.

Then, the system is asymptotically stable at the origin, that is, for all $\varepsilon>0$, *there exists* $\delta>0$ *such that, if* $\|\boldsymbol{x}_0\|_2\leq\delta$, *then* $\|\boldsymbol{x}(t)\|_2\leq\varepsilon$ *and* $\lim_{t\to\infty}\boldsymbol{x}(t)=0$. *Here,* V *is called a Lyapunov function.*

To find the NN-based controller satisfying the stability conditions in Theorem 5.1, we parameterize the controller and the Lyapunov function as $\boldsymbol{u}_{\boldsymbol{\phi}}$, $V_{\boldsymbol{\theta}}$, where $\boldsymbol{\phi}$ and $\boldsymbol{\theta}$ are trainable parameter vectors. Then, we define the supervised stabilization loss function as follows.

Definition 5.1 (Stabilization Loss)**.** *Consider a candidate potential function* $V_{\boldsymbol{\theta}}$ *and a controller* $\boldsymbol{u}_{\boldsymbol{\theta}}$ *for the controlled system* (5.12). *The Lyapunov stabilization loss is defined as*

$$L(\boldsymbol{\phi},\boldsymbol{\theta})\triangleq\frac{1}{N}\sum_{i=1}^{N}\Big[\lambda_1\boldsymbol{u}_{\boldsymbol{\phi}}(\boldsymbol{x}_i)^{\intercal}\boldsymbol{R}\boldsymbol{u}_{\boldsymbol{\phi}}(\boldsymbol{x}_i)+\lambda_2\big(\mathcal{L}_{f_{u_{\boldsymbol{\phi}}}}V_{\boldsymbol{\theta}}(\boldsymbol{x}_i)\big)\big)^{+}+\lambda_3\big(-V_{\boldsymbol{\theta}}(\boldsymbol{x}_i)\big)^{+}\Big]+|V(\boldsymbol{0})|^2,\tag{5.13}$$

where $\lambda_{1,2,3}>0$ *are hyper-parameters representing the weight factors of different conditions,* $\boldsymbol{R}$ *is a positive definitely matrix measures the importance of different control components,* $(\cdot)^+$ *denotes the operation* $\max(0,\cdot)$, *and* $\{(\boldsymbol{x}_i)\}_{i=1}^N$ *is the dataset sampled from the state space.*

Then, we train the parameters $\boldsymbol{\phi},\boldsymbol{\theta}$ with the stabilization loss function to obtain the stabilization controller $\boldsymbol{u}_{\boldsymbol{\phi}}$, and the learned $V_{\boldsymbol{\theta}}$ plays a role of stability certificate when applying the learned control policy to the patients.

Although the previous learning-based control methods perform well in the deterministic system, the practicability for stabilizing ODEs is limited to the real-world scenarios where stochasticity and randomness are of ubiquitous presence. This naturally calls for developing stabilization control policies for stochastic differential equations (SDEs) as well. Here, we consider the general controlled system described by the following Iô SDEs:

$$\mathrm{d}\boldsymbol{x}(t)=\boldsymbol{f}\big(\boldsymbol{x}(t),\boldsymbol{u}_f(\boldsymbol{x})\big)\mathrm{d}t+\boldsymbol{g}\big(\boldsymbol{x}(t),\boldsymbol{u}_g(\boldsymbol{x})\big)\mathrm{d}\boldsymbol{B}_t,\quad \boldsymbol{x}\in\mathbb{R}^d,\tag{5.14}$$

where $\boldsymbol{f}\in\mathbb{R}^d$ is the drift function, $\boldsymbol{g}\in\mathbb{R}^{d\times r}$ is the diffusion function with $\mathbb{R}^{d\times r}$, $\boldsymbol{B}_t\in\mathbb{R}^r$ is a r-dimensional standard Brownian motion, and the controller is comprised of deterministic control $\boldsymbol{u}_f$ and stochastic control $\boldsymbol{u}_g$. Still, we aim at stabilizing the unstable zero solution related to the normal brain state in the DBS task. We consider the stochastic exponential stability in this case.

Theorem 5.2 ([67], Stochastic Exponential Stability)**.** *Suppose that there exist a function* $V\in C^2(\mathbb{R}^d;\mathbb{R}_+)$ *with* $V(\boldsymbol{0})=0$, *constants* $p>0,\varepsilon>0$, *and* $c\in\mathbb{R}$ *such that*

(i) $V \in C^2(\mathbb{R}^d, \mathbb{R}_+), V(\mathbf{0}) = 0$,
(ii) $\varepsilon \|\boldsymbol{x}\|^p \leq V(\boldsymbol{x})$,
(iii) $\mathcal{L}V(\boldsymbol{x}) \leq cV(\boldsymbol{x})$ *for all* $\boldsymbol{x} \neq 0$ *and* $t \geq 0$.

Then,

$$\limsup_{t\to\infty} \frac{1}{t} \log \|\boldsymbol{x}(t;t_0,\boldsymbol{x}_0)\| \leq \frac{c}{p} \ \ a.s. \tag{5.15}$$

Here, the Lie operator for SDEs is defined as

$$\mathcal{L}V(\boldsymbol{x}) = \nabla V(\boldsymbol{x})^\intercal \boldsymbol{f}\big(\boldsymbol{x},\boldsymbol{u}(\boldsymbol{x})\big) + \frac{1}{2}\mathrm{Tr}\big[\boldsymbol{g}^\intercal\big(\boldsymbol{x},\boldsymbol{u}(\boldsymbol{x})\big)\nabla^2 V(\boldsymbol{x})\boldsymbol{g}\big(\boldsymbol{x},\boldsymbol{u}(\boldsymbol{x})\big)\big]. \tag{5.16}$$

In particular, if $c < 0$, *the zero solution of Eq.* (5.14) *is exponentially stable almost surely.*

Similarly, to find the NN-based controller satisfying the sufficient conditions in Theorem 5.2, we parameterize the controller and the V function as $\boldsymbol{u}_{\boldsymbol{\phi}}$, $V_{\boldsymbol{\theta}}$. Since the conditions in Theorem 5.2 are much complicated, we design suitable NN structure such that some conditions of V are satisfied in advance. Specifically, we construct the neural potential function $V_{\boldsymbol{\theta}}$ by using the convex functions [1] such that it satisfies the positive definite condition, i.e. $V_{\boldsymbol{\theta}}(\boldsymbol{x}) \geq 0$ and $V_{\boldsymbol{\theta}}(\mathbf{0}) = 0$. Second-order differentiable activation functions are used to guarantee $V_{\boldsymbol{\theta}} \in C^2(\mathbb{R};\mathbb{R}_+)$. We add L^p regularization term $\varepsilon\|\boldsymbol{x}\|^p$ with $\varepsilon \ll 1$ to $V_{\boldsymbol{\theta}}$ such that $V_{\boldsymbol{\theta}}(\boldsymbol{x}) \geq \varepsilon\|\boldsymbol{x}\|^p$. Then, we train the parameters according to the exponential stabilization loss function as follows.

Definition 5.2 (Exponential Stabilization Loss)**.** *Consider a candidate function* $V_{\boldsymbol{\theta}}$ *and a controller* $\boldsymbol{u}_{\boldsymbol{\phi}}$ *for the controlled system* (5.14). *The exponential stabilization loss is defined as*

$$L(\boldsymbol{\phi},\boldsymbol{\theta}) \triangleq \frac{1}{N}\sum_{i=1}^{N}\big[\boldsymbol{u}_{\boldsymbol{\theta}}(\boldsymbol{x}_i)^\intercal R \boldsymbol{u}_{\boldsymbol{\theta}}(\boldsymbol{x}_i) + \lambda_1 \max\big(0, \mathcal{L}V_{\boldsymbol{\theta}}(\boldsymbol{x}_i) - cV_{\boldsymbol{\theta}}(\boldsymbol{x}_i)\big)\big], \tag{5.17}$$

where $\lambda_1 > 0$ *and* $\boldsymbol{R}$ *are the same as those in Definition* 5.1, $c < 0$ *is the exponential decay rate, and* $\{(\boldsymbol{x}_i)\}_{i=1}^N$ *is the dataset.*

As indicated in [22,33], the biological systems of networked oscillators incur individual variability. Generally, there are two ways of modeling the individual variability in the literature. The first way is to sample the core parameters determining the property of the biological systems from a distribution for each individual, and then fix the sampled parameters. The other way is to use the stochastic process driven by different noises to perturb such parameters, where the degree of the variability is determined by the correlation of the perturbed noises and the diffusion matrix of the stochastic process. Actually, these two kinds of individual variability can be integrated into the AI framework: Training AI controllers based on the sampled dynamics for the former way, and designing AI controllers in the setting of stochastic system according to Theorem 5.2 for the latter.

6 Concluding remarks and perspective

In the realm of deep brain stimulation, several promising avenues for further exploration emerge from our comprehensive review. Firstly, as real-world environmental conditions often feature cyclical variations, understanding the dynamics of oscillators within cyclic network topology and fluctuating natural frequency distributions holds substantial promise. By delving into the intricacies of these systems, we can uncover novel insights into how DBS interventions may be optimized to account for periodic disturbances, potentially leading to more effective treatment strategies for neurological disorders.

Secondly, a notable gap exists in the realm of rigorously theoretical validations for advancing event-triggered control and AI-optimal control methodologies in DBS. While these approaches show great potential for enhancing the precision and efficiency of stimulation protocols, their theoretical underpinnings require further elucidation. Addressing this gap is imperative to ensure the robustness and reliability of future DBS technologies, underscoring the critical necessity for advancements in this area.

Furthermore, the integration of our findings into a framework of dynamic modeling alongside real closed-looped DBS techniques holds significant promise for augmenting the clinical management of neurodegenerative disorders. By combining mathematical insights with real-time feedback mechanisms, clinicians can tailor DBS interventions more precisely to individual patient needs, leading to improved therapeutic outcomes and reduced side effects. This interdisciplinary approach represents a promising direction for future research and clinical translation in the field of DBS.

In conclusion, the avenues highlighted in our review underscore the importance of continued interdisciplinary collaboration and innovation in advancing mathematical approaches for DBS. By further exploring the dynamics of oscillators, addressing theoretical gaps in control methodologies, and integrating dynamic modeling with real-time feedback, we can enhance the efficacy and precision of DBS treatments for neurological disorders, ultimately improving patient outcomes and quality of life.

Acknowledgments

The author would like to thank Wei Dai and Xiaoge Bao for their kindly advices on neuroscience background.

W. Lin is supported by the NSFC (No. 11925103), by the IPSMEC (No. 2023ZKZD04), and by the STCSM (Nos. 22JC1401402, 22JC1402500, 2021SHZDZX0103).

References

[1] B. Amos, L. Xu, and J. Z. Kolter, *Input convex neural networks*, in: International Conference on Machine Learning, PMLR, 146–155, 2017.

[2] V. I. Arnold, *Ordinary Differential Equations*, Springer Science & Business Media, 1992.

[3] P. Ashwin, S. Coombes, and R. Nicks, *Mathematical frameworks for oscillatory network dynamics in neuroscience*, J. Math. Neurosci., 6:1–92, 2016.
[4] A. L. Benabid, S. Chabardes, J. Mitrofanis, and P. Pollak, *Deep brain stimulation of the subthalamic nucleus for the treatment of Parkinson's disease*, Lancet Neurol., 8(1):67–81, 2009.
[5] A. Berényi, M. Belluscio, D. Mao, and G. Buzsáki, *Closed-loop control of epilepsy by transcranial electrical stimulation*, Science, 337(6095):735–737, 2012.
[6] C. Bick, M. Goodfellow, C. R. Laing, and E. A. Martens, *Understanding the dynamics of biological and neural oscillator networks through exact mean-field reductions: A review*, J. Math. Neurosci., 10(1):9, 2020.
[7] E. Brown, J. Moehlis, and P. Holmes, *On the phase reduction and response dynamics of neural oscillator populations*, Neural Comput., 16(4):673–715, 2004.
[8] J. Buhlmann, L. Hofmann, P. A. Tass, and C. Hauptmann, *Modeling of a segmented electrode for desynchronizing deep brain stimulation*, Front. Neuroeng., 4:15, 2011.
[9] E. Bullmore and O. Sporns, *Complex brain networks: Graph theoretical analysis of structural and functional systems*, Nat. Rev. Neurosci., 10(3):186–198, 2009.
[10] H. Cagnan et al., *Stimulating at the right time: Phase-specific deep brain stimulation*, Brain, 140(1):132–145, 2017.
[11] Y.-C. Chang, N. Roohi, and S. Gao, *Neural Lyapunov control*, in: Proceedings of the 33rd International Conference on Neural Information Processing Systems, Curran Associates Inc., 3245–3254, 2019.
[12] K. Chauhan, A. B. Neiman, and P. A. Tass, *Synaptic reorganization of synchronized neuronal networks with synaptic weight and structural plasticity*, PLoS Comput. Biol., 20(7):e1012261, 2024.
[13] Y. Che, T. Yang, R. Li, H. Li, C. Han, J. Wang, and X Wei, *Desynchronization in an ensemble of globally coupled chaotic bursting neuronal oscillators by dynamic delayed feedback control*, Int. J. Mod. Phys. B, 29(01):1450235, 2015.
[14] K.-H. S. Chen and R. Chen, *Invasive and noninvasive brain stimulation in Parkinson's disease: Clinical effects and future perspectives*, Clin. Pharmacol. Ther., 106(4):763–775, 2019.
[15] L. Chen, L. Xu, and C. Li, *Bursting, beating, and chaos in an excitable membrane model*, Acta Phys. Sin., 65(24):240701, 2016.
[16] T. Chen and H. Chen, *Universal approximation to nonlinear operators by neural networks with arbitrary activation functions and its application to dynamical systems*, IEEE Trans. Neural Netw., 6(4):911–917, 1995.
[17] C. Dawson, S. Gao, and C. Fan, *Safe control with learned certificates: A survey of neural Lyapunov, barrier, and contraction methods for robotics and control*, IEEE Trans. Robot., 39(3):1749–1767, 2023.
[18] C. de Hemptinne, E. S. Ryapolova-Webb, E. L. Air, P. A. Garcia, K. J. Miller, J. G. Ojemann, J. L. Ostrem, N. B. Galifianakis, and P. A. Starr, *Exaggerated phase-amplitude coupling in the primary motor cortex in Parkinson disease*, Proc. Natl. Acad. Sci. USA, 110(12):4780–4785, 2013.
[19] C. de Hemptinne, N. C. Swann, J. L. Ostrem, E. S. Ryapolova-Webb, M. S. Luciano, N. B. Galifianakis, and P. A. Starr, *Therapeutic deep brain stimulation reduces cortical phase-amplitude coupling in Parkinson's disease*, Nat. Neurosci., 18(5):779–786, 2015.
[20] M. R. DeLong and T. Wichmann, *Basal ganglia circuits as targets for neuromodulation in Parkinson disease*, JAMA Neurol., 72(11):1354–1360, 2015.
[21] J.-M. Deniau, B. Degos, C. Bosch, and N. Maurice, *Deep brain stimulation mechanisms: Beyond the concept of local functional inhibition*, Eur. J. Neurosci., 32(7):1080–1091, 2010.
[22] G. Drion, T. O'Leary, and E. Marder, *Ion channel degeneracy enables robust and tunable neuronal*

firing rates, Proc. Natl. Acad. Sci. USA, 112(38):E5361–E5370, 2015.
[23] B. Ermentrout, *Type i membranes, phase resetting curves, and synchrony*, Neural Computation, 8(5):979–1001, 1996.
[24] B. Ermentrout and A. Mahajan, *Simulating, analyzing, and animating dynamical systems: A guide to XPPAUT for researchers and students*, Appl. Mech. Rev., 56(4):B53–B53, 2003.
[25] B. Ermentrout, M. Pascal, and B. Gutkin, *The effects of spike frequency adaptation and negative feedback on the synchronization of neural oscillators*, Neural Comput., 13(6):1285–1310, 2001.
[26] D. Fan, Z. Wang, and Q. Wang, *Optimal control of directional deep brain stimulation in the parkinsonian neuronal network*, Commun. Nonlinear Sci. Numer. Simul., 36:219–237, 2016.
[27] Z. Feng, Y. Sun, L. Qian, Y. Qi, Y. Wang, C. Guan, and Y. Sun, *Design a novel BCI for neurorehabilitation using concurrent LFP and EEG features: A case study*, IEEE. Trans. Biomed. Eng., 69(5):1554–1563, 2022.
[28] R. FitzHugh, *Thresholds and plateaus in the Hodgkin-Huxley nerve equations*, J. Gen. Physiol., 43(5):867–896, 1960.
[29] R. FitzHugh, *Impulses and physiological states in theoretical models of nerve membrane*, Biophys. J., 1(6):445–466, 1961.
[30] J. E. Fleming, J. Orłowski, M. M. Lowery, and A. Chaillet, *Self-tuning deep brain stimulation controller for suppression of beta oscillations: Analytical derivation and numerical validation*, Front. Neurosci., 14:547800, 2020.
[31] J. Gao, B. Barzel, and A.-L. Barabási, *Universal resilience patterns in complex networks*, Nature, 530(7590):307–312, 2016.
[32] Q. Gao, M. Naumann, I. Jovanov, V. Lesi, K. Kamaravelu, W. M. Grill, and M. Pajic, *Model-based design of closed loop deep brain stimulation controller using reinforcement learning*, in: 2020 ACM/IEEE 11th International Conference on Cyber-Physical Systems (ICCPS), IEEE, 108–118, 2020.
[33] J. Garcia-Ojalvo, M. B. Elowitz, and S. H. Strogatz, *Modeling a synthetic multicellular clock: Repressilators coupled by quorum sensing*, Proc. Natl. Acad. Sci. USA, 101(30):10955–10960, 2004.
[34] L. Glass and M. C. Mackey, *From Clocks to Chaos: The Rhythms of Life*, Princeton University Press, 1988.
[35] V. Gradinaru, M. Mogri, K. R. Thompson, J. M. Henderson, and K. Deisseroth, *Optical deconstruction of parkinsonian neural circuitry*, Science, 324(5925):354–359, 2009.
[36] A. Guerra, V. López-Alonso, B. Cheeran, and A. Suppa, *Variability in non-invasive brain stimulation studies: Reasons and results*, Neurosci. Lett., 719:133330, 2020.
[37] B. S. Gutkin, G. B. Ermentrout, and A. D. Reyes, *Phase-response curves give the responses of neurons to transient inputs*, J. Neurophysiol., 94(2):1623–1635, 2005.
[38] A. Haddock, A. Velisar, J. Herron, H. Bronte-Stewart, and H. J. Chizeck, *Model predictive control of deep brain stimulation for parkinsonian tremor*, in: 2017 8th International IEEE/EMBS Conference on Neural Engineering (NER), IEEE, 358–362, 2017.
[39] I. Haidar, W. Pasillas-Lépine, A. Chaillet, E. Panteley, S. Palfi, and S. Senova, *Closed-loop firing rate regulation of two interacting excitatory and inhibitory neural populations of the basal ganglia*, Biol. Cybern., 110:55–71, 2016.
[40] K. D. Harris, *Neural signatures of cell assembly organization*, Nat. Rev. Neurosci., 6(5):399–407, 2005.
[41] S. Haufe, S. Dähne, and V. V. Nikulin, *Dimensionality reduction for the analysis of brain oscillations*, NeuroImage, 101:583–597, 2014.
[42] Y. Hayashi, T. Mishima, S. Fujioka, T. Morishita, T. Inoue, S. Nagamachi, and Y. Tsuboi,

Unilateral GPi-DBS improves ipsilateral and axial motor symptoms in Parkinson's disease as evidenced by a brain perfusion single photon emission computed tomography study, Front. Hum. Neurosci., 16:888701, 2022.

[43] S. He et al., *Beta-triggered adaptive deep brain stimulation during reaching movement in Parkinson's disease*, Brain, 146(12):5015–5030, 2023.

[44] D. O. Hebb, *The Organization of Behavior: A Neuropsychological Theory*, Psychology Press, 2005.

[45] W. P. M. H. Heemels, K. H. Johansson, and P. Tabuada, *An introduction to event-triggered and self-triggered control*, in: 2012 IEEE 51st IEEE Conference on Decision and Control (CDC), IEEE, 3270–3285, 2012.

[46] J. L. Hindmarsh and R. M. Rose, *A model of the nerve impulse using two first-order differential equations*, Nature, 296(5853):162–164, 1982.

[47] A. L. Hodgkin, *The local electric changes associated with repetitive action in a non-medullated axon*, J. Physiol 107(2):165–181, 1948.

[48] A. L. Hodgkin and A. F. Huxley, *A quantitative description of membrane current and its application to conduction and excitation in nerve*, J. Physiol., 117(4):500, 1952.

[49] E. M. Izhikevich, *Dynamical Systems in Neuroscience*, MIT Press, 2007.

[50] J. Jiang, Z.-G. Huang, T. P. Seager, W. Lin, C. Grebogi, A. Hastings, and Y.-C. Lai, *Predicting tipping points in mutualistic networks through dimension reduction*, Proc. Natl. Acad. Sci. USA, 115(4):E639–E647, 2018.

[51] M. D. Johnson, S. Miocinovic, C. C. McIntyre, and J. L. Vitek, *Mechanisms and targets of deep brain stimulation in movement disorders*, Neurotherapeutics, 5(2):294–308, 2008.

[52] D. Kaplan and L. Glass, *Understanding Nonlinear Dynamics*, Springer Science & Business Media, 2012.

[53] M. Kardar, *Statistical Physics of Particles*, Cambridge University Press, 2007.

[54] H. K. Khalil, *Nonlinear Systems*, Prentice Hall, 2002.

[55] B. Kralemann, M. Frühwirth, A. Pikovsky, M. Rosenblum, T. Kenner, J. Schaefer, and M. Moser, *In vivo cardiac phase response curve elucidates human respiratory heart rate variability*, Nat. Commun., 4(1):2418, 2013.

[56] D. Krylov, D. V. Dylov, and M. Rosenblum, *Reinforcement learning for suppression of collective activity in oscillatory ensembles*, Chaos, 30(3):033126, 2020.

[57] S. Kumar, H. Alawieh, F. S. Racz, R. Fakhreddine, and J. del R. Millán, *Transfer learning promotes acquisition of individual BCI skills*, PNAS Nexus, 3(2):76, 2024.

[58] E. Laurence, N. Doyon, L. J. Dubé, and P. Desrosiers, *Spectral dimension reduction of complex dynamical networks*, Phys. Rev. X, 9(1):011042, 2019.

[59] H. S. Lee, B. J. Kim, and H. J. Park, *Stability of twisted states in power-law-coupled Kuramoto oscillators on a circle with and without time delay*, Phys. Rev. E, 109(6):064203, 2024.

[60] F. L. Lewis, D. Vrabie, and V. L. Syrmos, *Optimal Control*, John Wiley & Sons, 2012.

[61] Z. Liang, Z. Luo, K. Liu, J. Qiu, and Q. Liu, *Online learning Koopman operator for closed-loop electrical neurostimulation in epilepsy*, IEEE J. Biomed. Health Inform., 27(1):492–503, 2022.

[62] S. Little and P. Brown, *Debugging adaptive deep brain stimulation for Parkinson's disease*, Mov. Disord., 35(4):555–561, 2020.

[63] S. Little et al., *Adaptive deep brain stimulation in advanced Parkinson disease*, Ann. Neurol., 74(3):449–457, 2013.

[64] S. Little et al., *Bilateral adaptive deep brain stimulation is effective in Parkinson's disease*, J. Neurol. Neurosurg. Psychiatry, 87(7):717–721, 2016.

[65] C. Liu, G. Zhao, J. Wang, H. Wu, H. Li, C. Fietkiewicz, and K. A. Loparo, *Neural network-*

based closed-loop deep brain stimulation for modulation of pathological oscillation in Parkinson's disease, IEEE Access, 8:161067–161079, 2020.

[66] T. B. Luke, E. Barreto, and P. So, *Macroscopic complexity from an autonomous network of networks of theta neurons*, Front. Comput. Neurosci., 8:145, 2014.

[67] X. Mao, *Stochastic Differential Equations and Applications*, Elsevier, 2007.

[68] A. C. Meidahl, G. Tinkhauser, D. M. Herz, H. Cagnan, J. Debarros, and P. Brown, *Adaptive deep brain stimulation for movement disorders: The long road to clinical therapy*, Mov. Disord., 32(6):810–819, 2017.

[69] T. Merk, V. Peterson, R. Köhler, S. Haufe, R. M. Richardson, and W.-J. Neumann, *Machine learning based brain signal decoding for intelligent adaptive deep brain stimulation*, Exp. Neurol., 351:113993, 2022.

[70] D. Meunier, R. Lambiotte, and E. T. Bullmore, *Modular and hierarchically modular organization of brain networks*, Front. Neurosci., 4:7572, 2010.

[71] C. Meunier and I. Segev, *Playing the devil's advocate: Is the Hodgkin-Huxley model useful?* Trends Neurosci., 25(11):558–563, 2002.

[72] B. Monga, D. Wilson, T. Matchen, and J. Moehlis, *Phase reduction and phase-based optimal control for biological systems: A tutorial*, Biol. Cybern., 113(1):11–46, 2019.

[73] G. Montaseri, M. J. Yazdanpanah, A. Pikovsky, and M. Rosenblum, *Synchrony suppression in ensembles of coupled oscillators via adaptive vanishing feedback*, Chaos, 23(3):033122, 2013.

[74] C. Morris and H. Lecar, *Voltage oscillations in the barnacle giant muscle fiber*, Biophys. J., 35(1):193–213, 1981.

[75] S. F. Muldoon, F. Pasqualetti, S. Gu, M. Cieslak, S. T. Grafton, J. M. Vettel, and D. S. Bassett, *Stimulation-based control of dynamic brain networks*, PLoS Comput. Biol., 12(9):e1005076, 2016.

[76] J. Nagumo, S. Arimoto, and S. Yoshizawa, *An active pulse transmission line simulating nerve axon*, Proc. IRE, 50(10):2061–2070, 1962.

[77] T. Netoff, M. A. Schwemmer, and T. J. Lewis, *Experimentally estimating phase response curves of neurons: Theoretical and practical issues*, in: Phase Response Curves in Neuroscience. Springer Series in Computational Neuroscience, Vol. 6, Springer, 95–129, 2012.

[78] A. J. Nevado Holgado, J. R. Terry, and R. Bogacz, *Conditions for the generation of beta oscillations in the subthalamic nucleus-globus pallidus network*, J. Neurosci., 30(37):12340–12352, 2010.

[79] M. A. Nowak, *Five rules for the evolution of cooperation*, Science, 314(5805):1560–1563, 2006.

[80] E. Ott and T. M. Antonsen, *Low dimensional behavior of large systems of globally coupled oscillators*, Chaos, 18(3):037113, 2008.

[81] P. A. Parrilo, *Structured Semidefinite Programs and Semialgebraic Geometry Methods in Robustness and Optimization*, PhD Thesis, California Institute of Technology, 2000.

[82] W. Pasillas-Lépine, I. Haidar, A. Chaillet, and E. Panteley, *Closed-loop deep brain stimulation based on firing-rate regulation*, in: 2013 6th International IEEE/EMBS Conference on Neural Engineering (NER), IEEE, 166–169, 2013.

[83] M. Peralta, P. Jannin, and J. S. H. Baxter, *Machine learning in deep brain stimulation: A systematic review*, Artif. Intell. Med., 122:102198, 2021.

[84] D. Piña-Fuentes, J. M. C. van Dijk, J. C. van Zijl, H. R. Moes, T. van Laar, D. L. M. Oterdoom, S. Little, P. Brown, and M. Beudel, *Acute effects of adaptive deep brain stimulation in Parkinson's disease*, Brain Stimul., 13(6):1507–1516, 2020.

[85] O. V. Popovych, C. Hauptmann, and P. A. Tass, *Effective desynchronization by nonlinear delayed feedback*, Phys. Rev. Lett., 94(16):164102, 2005.

[86] O. V. Popovych, C. Hauptmann, and P. A. Tass, *Control of neuronal synchrony by nonlinear*

delayed feedback, Biol. Cybern., 95(1):69–85, 2006.
[87] O. V. Popovych and P. A. Tass, *Synchronization control of interacting oscillatory ensembles by mixed nonlinear delayed feedback*, Phys. Rev. E, 82(2):026204, 2010.
[88] K. Pyragas, O.V. Popovych, and P. A. Tass, *Controlling synchrony in oscillatory networks with a separate stimulation-registration setup*, EPL, 80(4):40002, 2007.
[89] Y. Qin, D. S. Bassett, and F. Pasqualetti, *Vibrational control of cluster synchronization: Connections with deep brain stimulation*, in: 2022 IEEE 61st Conference on Decision and Control (CDC), IEEE, 655–661, 2022.
[90] I. Ratas and K. Pyragas, *Effect of high-frequency stimulation on nerve pulse propagation in the FitzHugh-Nagumo model*, Nonlinear Dyn., 67:2899–2908, 2012.
[91] I. Ratas and K. Pyragas, *Controlling synchrony in oscillatory networks via an act-and-wait algorithm*, Phys. Rev. E, 90(3):032914, 2014.
[92] I. Ratas and K. Pyragas, *Eliminating synchronization in bistable networks*, Nonlinear Dyn., 83:1137–1151, 2016.
[93] M. Rehan and K.-S. Hong, *Modeling and automatic feedback control of tremor: Adaptive estimation of deep brain stimulation*, PLoS One, 8(4):e62888, 2013.
[94] A. Rényi, *Probability Theory*, Courier Corporation, 2007.
[95] S. Revzen and J. M. Guckenheimer, *Estimating the phase of synchronized oscillators*, Phys. Rev. E, 78(5):051907, 2008.
[96] M. G. Rizzone et al., *Long-term outcome of subthalamic nucleus DBS in Parkinson's disease: From the advanced phase towards the late stage of the disease?* Parkinsonism Relat. Disord., 20(4):376–381, 2014.
[97] M. C. Rodriguez-Oroz et al., *Bilateral deep brain stimulation in Parkinson's disease: A multicentre study with 4 years follow-up*, Brain, 128(10):2240–2249, 2005.
[98] R. M. Rose and J. L. Hindmarsh, *Bursting, beating, and chaos in an excitable membrane model*, Biophys. J., 47(3):357–366, 1985.
[99] R. M. Rose and J. L. Hindmarsh, *The assembly of ionic currents in a thalamic neuron. I. The three-dimensional model*, Proc. Royal Soc. B., 237(1288):267–288, 1989.
[100] M. Rosenblum and A. Pikovsky, *Delayed feedback control of collective synchrony: An approach to suppression of pathological brain rhythms*, Phys. Rev. E, 70(4):041904, 2004.
[101] B. Rosin, M. Slovik, R. Mitelman, M. Rivlin-Etzion, S. N. Haber, Z. Israel, E. Vaadia, and H. Bergman, *Closed-loop deep brain stimulation is superior in ameliorating parkinsonism*, Neuron, 72(2):370–384, 2011.
[102] J. E. Rubin and D. Terman, *High frequency stimulation of the subthalamic nucleus eliminates pathological thalamic rhythmicity in a computational model*, J. Comput. Neurosci., 16:211–235, 2004.
[103] L. Rui, H. Nejati, and N.-M. Cheung, *Dimensionality reduction of brain imaging data using graph signal processing*, in: IEEE International Conference on Image Processing (ICIP), IEEE, 1329–1333, 2016.
[104] S. Russell, *Human Compatible: AI and the Problem of Control*, Penguin, 2019.
[105] L. Salfenmoser and K. Obermayer, *Optimal control of a Wilson-Cowan model of neural population dynamics*, Chaos, 33(4):043135, 2023.
[106] A. A. Sarma, B. Crocker, S. S. Cash, and W. Truccolo, *A modular, closed-loop platform for intracranial stimulation in people with neurological disorders*, in: 2016 38th Annual International Conference of the IEEE Engineering in Medicine and Biology Society (EMBC), IEEE, 3139–3142, 2016.
[107] S. S. Sastry and A. Isidori, *Adaptive control of linearizable systems*, IEEE Trans. Automat.

Contr., 34(11):1123–1131, 1989.
[108] J. Schulman, F. Wolski, P. Dhariwal, A. Radford, and O. Klimov, *Proximal policy optimization algorithms*, ArXiv:1707.06347, 2017.
[109] R. Schulz, C. Gerloff, and F. C. Hummel, *Non-invasive brain stimulation in neurological diseases*, Neuropharmacology, 64:579–587, 2013.
[110] J. T. C. Schwabedal and H. Kantz, *Optimal extraction of collective oscillations from unreliable measurements*, Phys. Rev. Lett., 116(10):104101, 2016.
[111] A. A. Selivanov, J. Lehnert, T. Dahms, P. Hövel, A. L. Fradkov, and E. Schöll, *Adaptive synchronization in delay-coupled networks of Stuart-Landau oscillators*, Phys. Rev. E, 85(1):016201, 2012.
[112] C. Sherrington, *The integrative action of the nervous system*, J. Nerv. Ment. Dis., 34(12):801–802, 1907.
[113] R. B. Stein, *A theoretical analysis of neuronal variability*, Biophys. J., 5(2):173–194, 1965.
[114] R. B. Stein and A. L. Hodgkin, *The frequency of nerve action potentials generated by applied currents*, Proc. Royal Soc. B, 167(1006):64–86, 1967.
[115] E. M. Stein and R. Shakarchi, *Complex Analysis, Vol. II*, Princeton University Press, 2010.
[116] K. M. Stiefel, B. S. Gutkin, and T. J. Sejnowski, *Cholinergic neuromodulation changes phase response curve shape and type in cortical pyramidal neurons*, PLoS One, 3(12):e3947, 2008.
[117] B. M. 't Hart et al., *Neuromatch academy: A 3-week, online summer school in computational neuroscience*, J. Open Source Educ., 5(49):118, 2022.
[118] A. Tamaševičius, E. Tamaševičiūtė, and G. Mykolaitis, *Feedback controller for destroying synchrony in an array of the FitzHugh-Nagumo oscillators*, Appl. Phys. Lett., 101(22), 2012.
[119] D. Terman, J. E. Rubin, A. C. Yew, and C. J. Wilson, *Activity patterns in a model for the subthalamopallidal network of the basal ganglia*, J. Neurosci., 22(7):2963–2976, 2002.
[120] W. J. Terrell, *Stability and Stabilization: An Introduction*, Princeton University Press, 2009.
[121] V. Thibeault, G. St-Onge, L. J. Dubé, and P. Desrosiers, *Threefold way to the dimension reduction of dynamics on networks: An application to synchronization*, Phys. Rev. Res., 2(4):043215, 2020.
[122] G. Tinkhauser, A. Pogosyan, S. Little, M. Beudel, D. M. Herz, H. Tan, and P. Brown, *The modulatory effect of adaptive deep brain stimulation on beta bursts in Parkinson's disease*, Brain, 140(4):1053–1067, 2017.
[123] P. J. Uhlhaas and W. Singer, *Neural synchrony in brain disorders: Relevance for cognitive dysfunctions and pathophysiology*, Neuron, 52(1):155–168, 2006.
[124] K. R. Wan, T. Maszczyk, A. A. Q. See, J. Dauwels, and N. K. K. King, *A review on microelectrode recording selection of features for machine learning in deep brain stimulation surgery for Parkinson's disease*, Clin. Neurophysiol., 130(1):145–154, 2019.
[125] K. Wang, L. Yang, S. Zhou, and W. Lin, *Desynchronizing oscillators coupled in multi-cluster networks through adaptively controlling partial networks*, Chaos, 33(9):091101, 2023.
[126] G. Weerasinghe, B. Duchet, H. Cagnan, P. Brown, C. Bick, and R. Bogacz, *Predicting the effects of deep brain stimulation using a reduced coupled oscillator model*, PLoS Comput. Biol., 15(8):e1006575, 2019.
[127] A. T. Winfree, *The Geometry of Biological Time*, Springer-Verlag, 1980.
[128] T. Xie, J. Vigil, E. MacCracken, A. Gasparaitis, J. Young, W. Kang, J. Bernard, P. Warnke, and U. J. Kang, *Low-frequency stimulation of STN-DBS reduces aspiration and freezing of gait in patients with PD*, Neurology, 84(4):415–420, 2015.
[129] Y. Yang, S. Qiao, O. G. Sani, J. I. Sedillo, B. Ferrentino, B. Pesaran, and M. M. Shanechi, *Modelling and prediction of the dynamic responses of large-scale brain networks during direct electrical*

stimulation, Nat. Biomed. Eng., 5(4):324–345, 2021.
[130] Y. Zang, S. Hong, and E. De Schutter, *Firing rate-dependent phase responses of purkinje cells support transient oscillations*, Elife, 9:e60692, 2020.
[131] J. Zhang, Q. Zhu, and W. Lin, *Neural stochastic control*, Adv. Neural Inf. Process. Syst., 35:9098–9110, 2022.
[132] S. Zhou, P. Ji, Q. Zhou, J. Feng, J. Kurths, and W. Lin, *Adaptive elimination of synchronization in coupled oscillator*, New J. Phys., 19(8):083004, 2017.
[133] S. Zhou, Y.-C. Lai, and W. Lin, *Stochastically adaptive control and synchronization: From globally one-sided Lipschitzian to only locally Lipschitzian systems*, SIAM J. Appl. Dyn. Syst., 21(2):932–959, 2022.
[134] S. Zhou and W. Lin, *Eliminating synchronization of coupled neurons adaptively by using feedback coupling with heterogeneous delays*, Chaos, 31(2):023114, 2021.
[135] C. Zhou, L. Zemanová, G. Zamora, C. C. Hilgetag, and J. Kurths, *Hierarchical organization unveiled by functional connectivity in complex brain networks*, Phys. Rev. Lett., 97(23):238103, 2006.